Elemental Water Impact Test: Phase 2 36-inch Aluminum Tank Head

Gregory J. Vassilakos
Analytical Mechanics Associates, Inc., Hampton, Virginia

December 2014

NASA STI Program . . . in Profile

Since its founding, NASA has been dedicated to the advancement of aeronautics and space science. The NASA scientific and technical information (STI) program plays a key part in helping NASA maintain this important role.

The NASA STI program operates under the auspices of the Agency Chief Information Officer. It collects, organizes, provides for archiving, and disseminates NASA's STI. The NASA STI program provides access to the NTRS Registered and its public interface, the NASA Technical Reports Server, thus providing one of the largest collections of aeronautical and space science STI in the world. Results are published in both non-NASA channels and by NASA in the NASA STI Report Series, which includes the following report types:

- TECHNICAL PUBLICATION. Reports of completed research or a major significant phase of research that present the results of NASA Programs and include extensive data or theoretical analysis. Includes compilations of significant scientific and technical data and information deemed to be of continuing reference value. NASA counter-part of peer-reviewed formal professional papers but has less stringent limitations on manuscript length and extent of graphic presentations.

- TECHNICAL MEMORANDUM. Scientific and technical findings that are preliminary or of specialized interest, e.g., quick release reports, working papers, and bibliographies that contain minimal annotation. Does not contain extensive analysis.

- CONTRACTOR REPORT. Scientific and technical findings by NASA-sponsored contractors and grantees.

- CONFERENCE PUBLICATION. Collected papers from scientific and technical conferences, symposia, seminars, or other meetings sponsored or co-sponsored by NASA.

- SPECIAL PUBLICATION. Scientific, technical, or historical information from NASA programs, projects, and missions, often concerned with subjects having substantial public interest.

- TECHNICAL TRANSLATION. English-language translations of foreign scientific and technical material pertinent to NASA's mission.

Specialized services also include organizing and publishing research results, distributing specialized research announcements and feeds, providing information desk and personal search support, and enabling data exchange services.

For more information about the NASA STI program, see the following:

- Access the NASA STI program home page at http://www.sti.nasa.gov

- E-mail your question to help@sti.nasa.gov

- Phone the NASA STI Information Desk at 757-864-9658

- Write to:
  NASA STI Information Desk
  Mail Stop 148
  NASA Langley Research Center
  Hampton, VA 23681-2199

NASA/CR–2014-218667

Elemental Water Impact Test: Phase 2 36-inch Aluminum Tank Head

Gregory J. Vassilakos
Analytical Mechanics Associates, Inc., Hampton, Virginia

December 2014

Acknowledgments

The author would like to recognize Dr. Karen Lyle, Steve Gayle, and Dr. Peter Gage for developing the plan for the test series and arranging the set-up of the test facility and fabrication of the test article. The author would like to thank David Stegall for his exhaustive efforts in providing test data and troubleshooting problems with the instrumentation and data acquisition system.

Abstract

Spacecraft are being designed based on LS-DYNA simulations of water landing impacts. The Elemental Water Impact Test (EWIT) series was undertaken to assess the accuracy of LS-DYNA water impact simulations. EWIT Phase 2 featured a 36-inch aluminum tank head. The tank head was outfitted with one accelerometer, twelve pressure transducers, three string potentiometers, and four strain gages. The tank head was dropped from heights of 1 foot and 2 feet. The focus of this report is the correlation of analytical models against test data.

As a measure of prediction accuracy, peak responses from the baseline LS-DYNA model were compared to peak responses from the tests. The average absolute percentage deviations were as follows.

Average Absolute Percentage Deviations

Parameter	Average Absolute Percentage Deviation
Acceleration	24.2
Pressure	222.2
Deflection	29.2
Stress	15.5

The results for the tank head model demonstrated the following.

1. *LS-DYNA can provide reasonable predictions for acceleration, deflection, and stress time histories for a broad range of fluid-structure coupling parameters.*
2. *LS-DYNA acceleration, deflection, and stress time histories converge as mesh density increases.*
3. *LS-DYNA coupling pressure time histories are highly dependent on fluid-structure coupling parameters.*
4. *LS-DYNA coupling pressure time histories do not necessarily converge as mesh density increases.*

Table of Contents

List of Figures

List of Tables

1. Introduction

Spacecraft are being designed based on LS-DYNA [1] simulations of water landing impacts. The Elemental Water Impact Test (EWIT) series was undertaken to assess the accuracy of LS-DYNA water impact simulations. Phase 1 of the EWIT test series featured water drop tests of a 20-inch spherical penetrometer, and focused on acceleration and pressure measurements [2]. The focus of this report is Phase 2, which featured a 36-inch aluminum tank head with acceleration, pressure, deflection, and strain measurements. The tank head was dropped from heights of 1 foot and 2 feet.

2. Tests

2.1. Test Configuration

The conduct of the tests is described in a separate test report [3]. The drop tests were performed in a 15-foot above-ground swimming pool. The test pool was located inside a 24-foot above-ground swimming pool to catch any over splash. A foam pad existed under the floor of the inner pool to cushion the blow from bottom impacts. The test article was suspended above the test pool via a forklift. A line hanging from the test article was used to measure the drop height. The general set-up is illustrated in Figure 1.
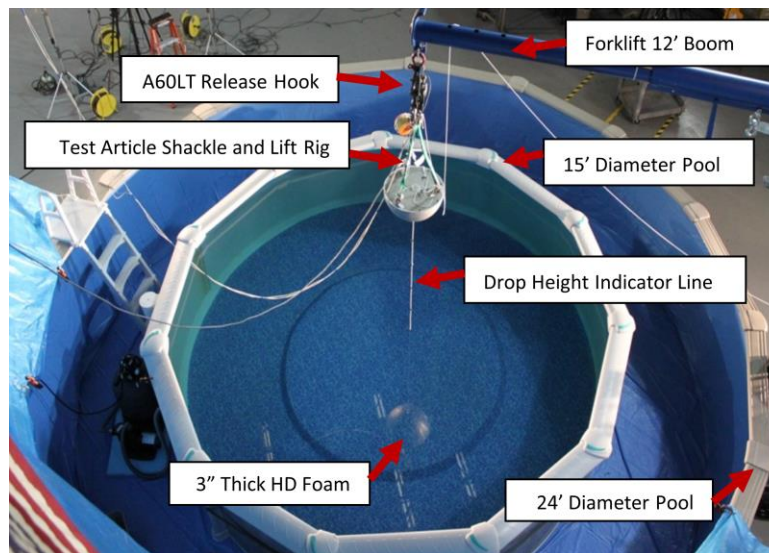
Figure 1. Test Set-Up

2.2. Test Article

The Phase 2 EWIT test article was an aluminum tank head. The diameter at the rim was approximately 36 inches, the radius of curvature at the center was approximately 34 inches, and the depth from the rim to the apex was approximately 7.7 inches. The test article is illustrated in Figure 2. The test article featured a cover plate and a dished tank

head. The cover plate was attached to the tank head via twelve fasteners. The tank head was machined to shell thickness of less than 0.1 inches across most of its area to ensure that significant deformation occurred during the water impacts. Due to limitations in the precision of the machining process, the thickness was highly non-uniform. The distribution of the thickness is illustrated in Figure 3. The tank head was manufactured from Aluminum 5083-O, which has a yield strength of 18,000 psi. The total weight of the test article was 117.5 lb.
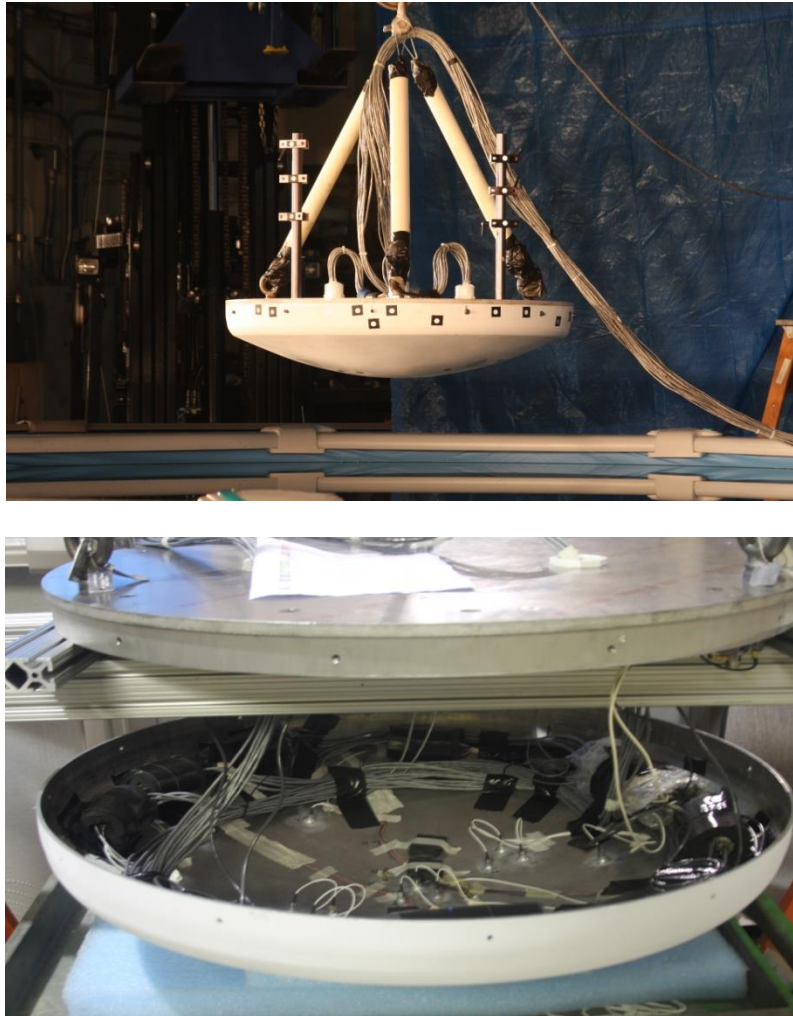
Figure 2. 36-inch Tank Head
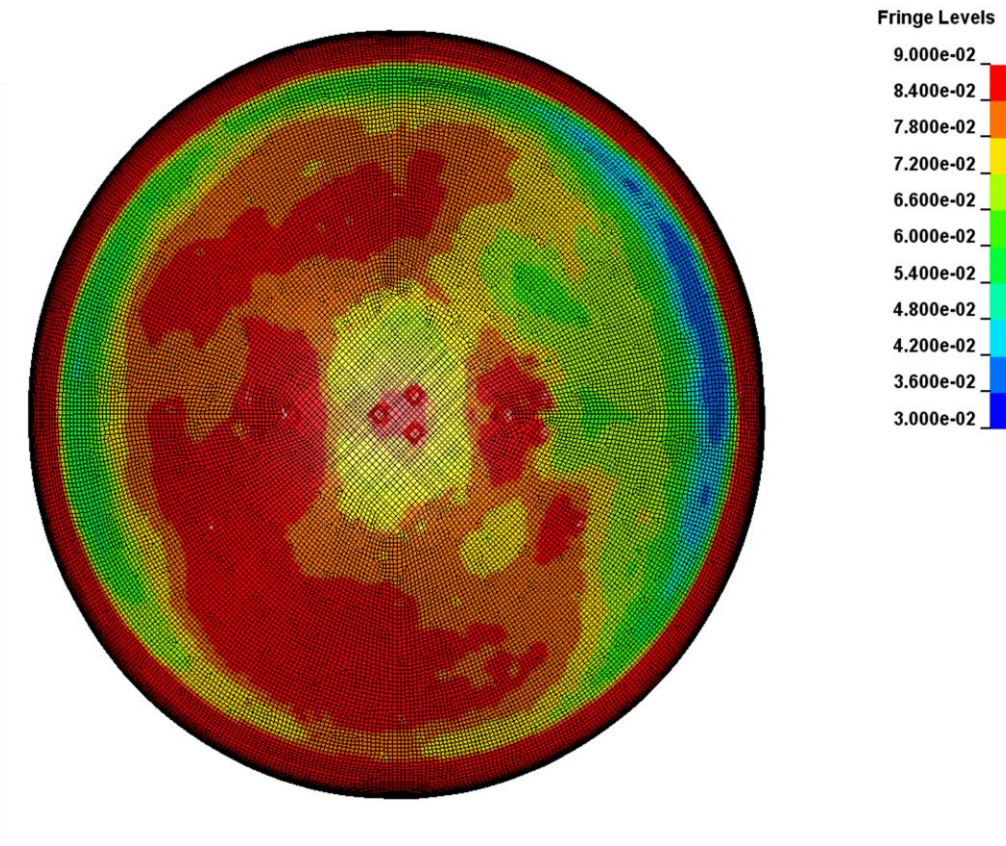
Figure 3. 36-inch Tank Head Thickness Distribution

The test article was outfitted with one accelerometer, twelve pressure transducers, three string potentiometers (A.K.A. string pots), and four strain gages. The arrangement of the sensors is illustrated in Figure 4. The accelerometer was mounted to the cover plate bolting ring near the –Z edge. This location was chosen because it was relatively stiff and less prone to vibratory noise. The pressure transducers were arranged in groups of three in order to provide multiple readings from transducers in the same vicinity in order to confirm the repeatability of the measurements. The string pots featured a reel mounted to the cover plate from which extended a string that attached to a hook on the tank head. The strain gages were rectangular rosettes. Each rosette featured two strain gages at right angles plus a third strain gage aligned 45 degrees relative to the other two.
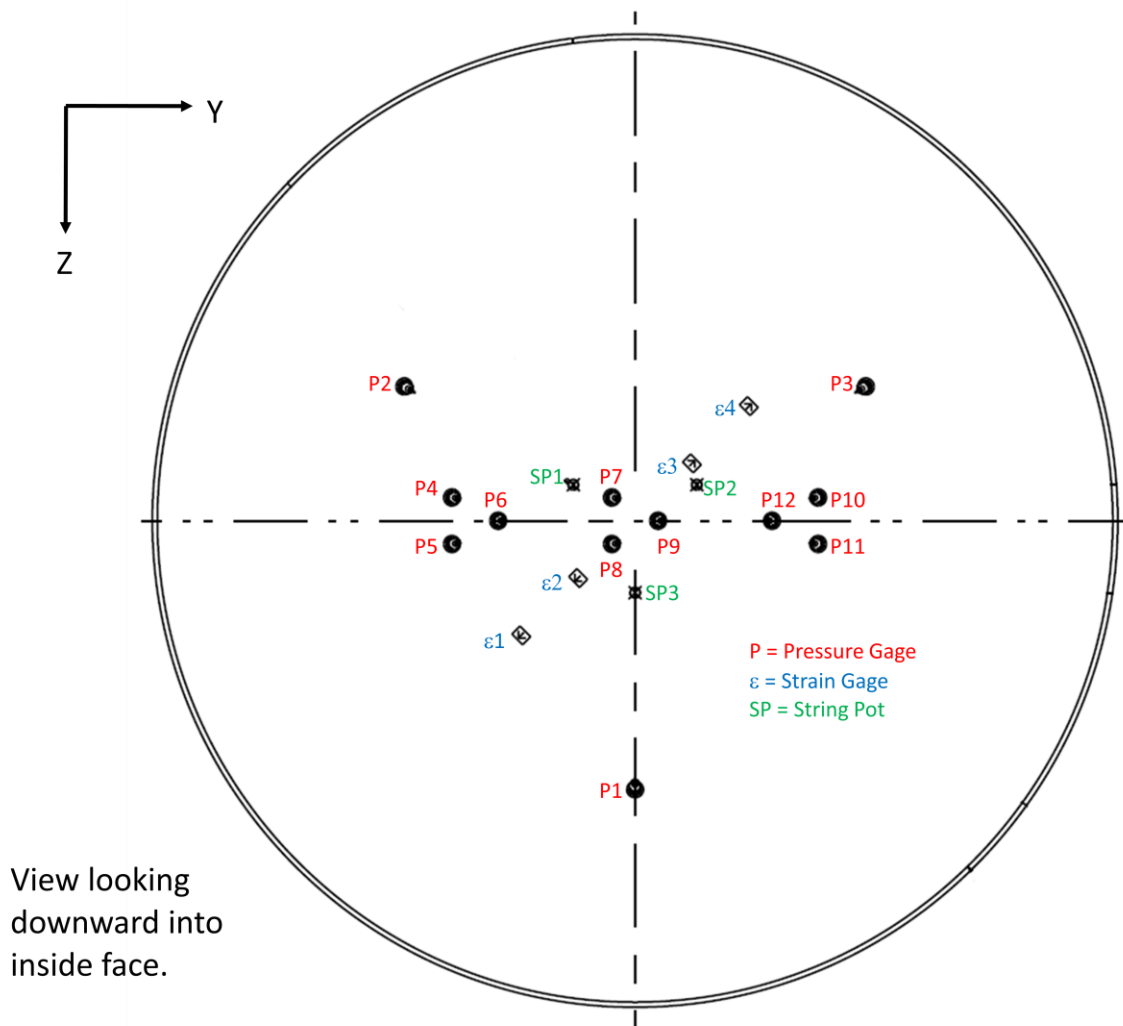
Figure 4. Sensor Arrangement

2.3. Test Matrix

Water impact tests were performed at drop heights of 1 foot and 2 feet. Table 1 lists the tests. Data from two tests at each drop height was used for comparison against simulations.

Table 1. Test Matrix

Test	Drop Height (ft)	Comments
7/26 Drop 1	1	First test for testing instrumentation.
8/27 Drop 1	1	Scaling problem with stress data. Acceleration data used for comparison with simulations.
8/30 Drop 1	1	Data used for comparison with simulations.
8/30 Drop 2	2	Data used for comparison with simulations.
8/30 Drop 3	2	Data used for comparison with simulations.
9/10 Drop 1	1	Acceleration data clipped. Pressure, deflection, and strain data used for comparison with simulations.
9/10 Drop 2	1	Acceleration data clipped.
9/10 Drop 3	1	Acceleration data clipped.
9/10 Drop 4	2	Acceleration data clipped.
9/10 Drop 5	2	Acceleration data clipped.
9/10 Drop 6	2	Acceleration data clipped.

3. LS-DYNA Model

The LS-DYNA model of the tank head featured shell elements for the tank head and the cover plate. Solid elements were used for the bolting ring that connected the cover plate to the tank head. All shell elements were fully integrated (ELFORM = 16). In order to track inelastic behavior during bending, the elements of the tank head featured ten integration points through the thickness. Lobatto integration was used so that the first and last integration points were exactly on the inner and outer surface. The cover plate was expected to remain elastic and featured Gauss integration with just two integration points through the thickness. The solid elements of the bolting ring were under-integrated (ELFORM=1).

The nominal element size for the tank head was 0.2 inches. The nominal element size for the cover plate was 1 inch. The material properties for the tank head are listed in Table 2. All material was aluminum. Only the tank head had an elastic-plastic material model. The density of the bolting ring was adjusted to achieve the proper total weight for the model. No damping was applied to the structural model. The mesh is illustrated in Figure 5.

Table 2. Tank Head Model Material Properties

Material Parameter	Tank Head	Cover Plate	Bolting Ring
Material	Aluminum	Aluminum	Aluminum
Thickness (in)	Variable	0.5	-
Density (lb/in3/g)	2.53E-4	2.53E-4	2.491E-4
Elastic Modulus (psi)	10.2E6	10.2E6	10.2E6
Poisson's Ratio	0.33	0.33	0.33
Yield Stress (psi)	18000.	-	-
Tangent Modulus (psi)	10.2E4	-	-
# Integration Points	10 (Lobatto)	2 (Gauss)	-
Damping	None	None	None

The cover plate and the tank head were each attached to the bolting ring via twelve sets of beam elements representing fasteners. The beams extended through the depth of one solid element of the bolting ring to provide stiffness to resist bending rotations. Rigid spiders were added at the shell end of the beams to avoid having no stiffness for axial rotations. The beams were steel and were 3/8-inch diameter for the cover plate attachment and ¼-inch diameter for the tank head attachment. The beam connections are described in Figure 5. Contact surfaces were defined between the bolting ring and both the cover plate and the tank head for the water impact simulations, but not for the modal analysis.

Model shown with cover cutaway for clarity.

Node at top end of beam plus three nearby nodes connected as rigid body.

Cover Plate

Node at outer end of beam plus four nearby nodes connected as rigid body.

Bolting Ring

Fastener represented as 3/8" Ø steel beam.

Fastener represented as 1/4" Ø steel beam.

Tank Head
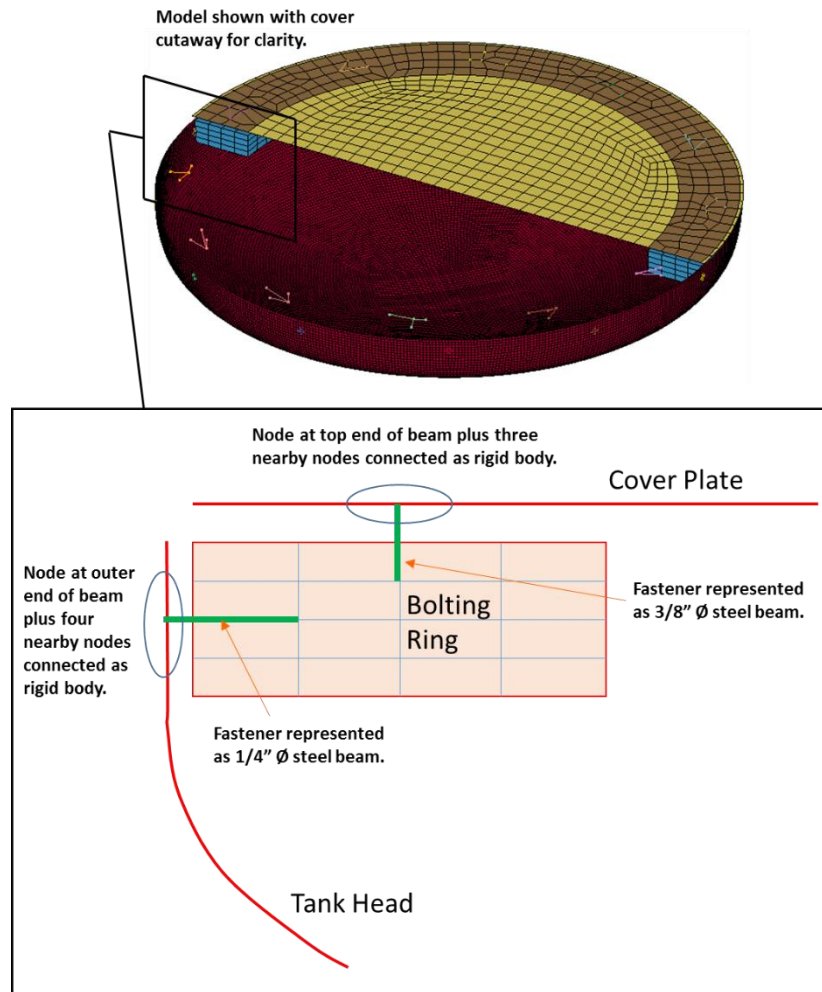
Figure 5. Test Article Finite Element Mesh and Bolted Connection Modeling

The fluid was modeled using the multi-material Arbitrary Lagrange in Euler (ALE) formulation in LS-DYNA. The fluid mesh is illustrated in Figure 6. The fluid element size in way of the initial impact was approximately 0.2 inches. The fluid mesh diameter was 60 inches. The air above the water had a height of 3 inches. The water had a depth of 21 inches. A layer of ambient elements existed at the outer perimeter and bottom of the fluid mesh. The ambient elements mimic a much larger body of water by allowing material to move in and out of the mesh while holding the pressure constant at the boundary. Both the air and water were modeled with equations of state. The fluid-structure coupling was defined for the tank head to interact with only the water, not the air. The air was initialized to one atmosphere. The water was initialized to one atmosphere plus hydrostatic pressure. The LS-DYNA cards that define the coupling stiffness, material properties, and initial conditions are provided in Appendix A.
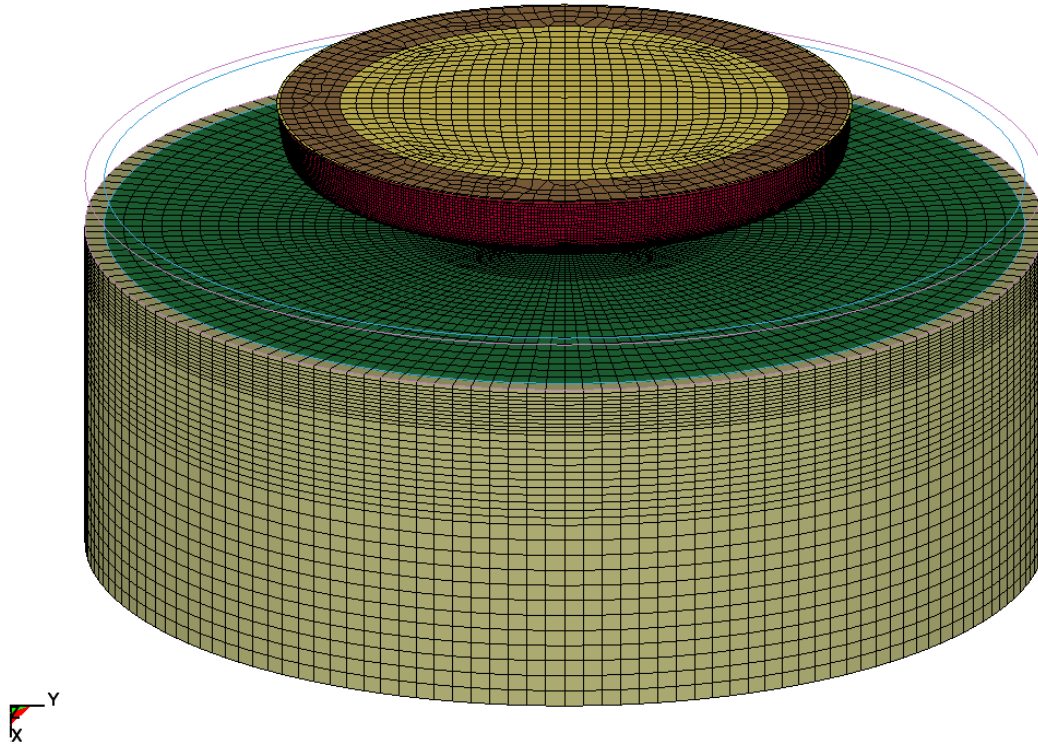
Figure 6. Fluid Mesh

LS-DYNA features a penalty method for fluid-structure coupling. Artificial springs are inserted between the fluid and the structure whenever the fluid penetrates the structural boundary. Damping can be added in parallel to the coupling springs. The baseline model utilized a fluid-structure coupling stiffness curve referred to as Curve 11, which featured a coupling pressure of 200 psi at a penetration distance of 0.02 inches. Damping of the fluid-structure coupling surface was set to 50% critical, DAMP = 0.5. The default was used for the minimum volume fraction for fluid coupling, FRCMIN = 0.5.

4. Modal Vibration Test

A modal vibration test was performed with the tank head hanging from three support cables [4]. The tests set-up is illustrated in Figure 7. For the test, the tank head was outfitted with a radial line of accelerometers on the cover plate and on the tank head. The test article was excited by hitting the cover plate with a hammer at a point approximately two-thirds of the radius from the center. The first three modes determined from the test are illustrated in Figure 8.

8
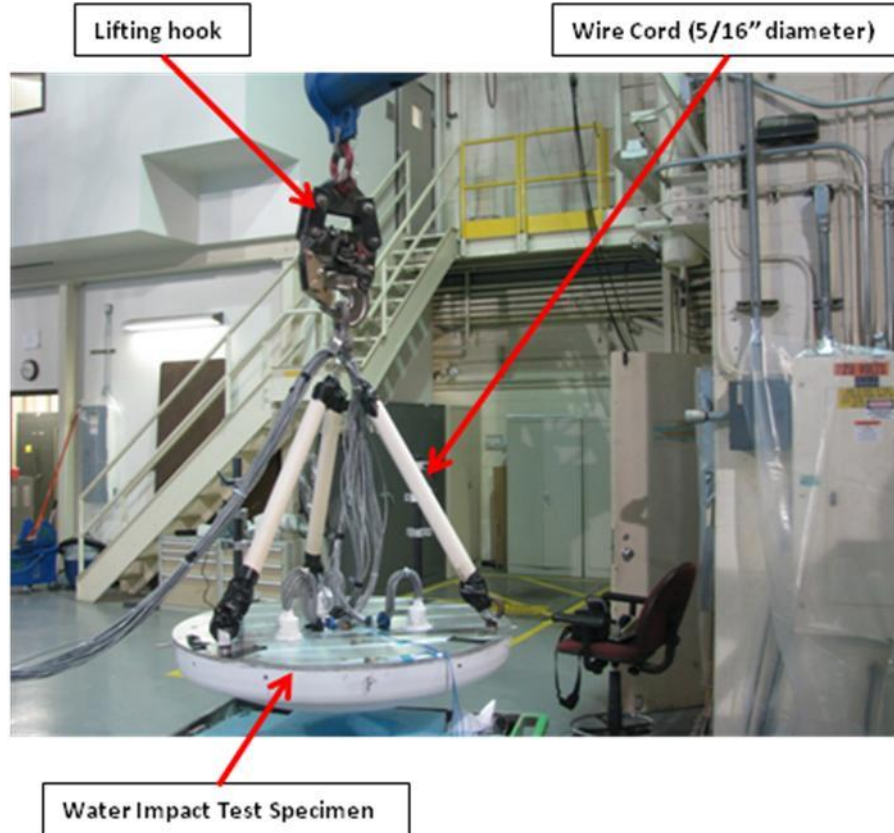
Figure 7. Modal Test Set-Up

Mode 1 – 168 Hz
Flexure of Cover.

Mode 2 – 259 Hz
Flexure of Cover & Dish.

Mode 3 – 310 Hz
Flexure of Cover.
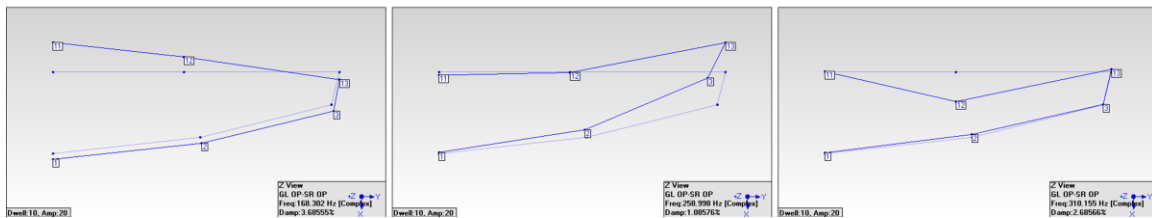
Figure 8. First Three Modes from Modal Test

An Eigen mode vibration analysis was performed using the implicit solver in LS-DYNA. For the Eigen solution, three beam elements were added to represent the cables. The model was restrained at the top of the cables. The flexural modes of the model are illustrated in Figure 9 and are compared to the test modes in Table 3. The frequencies of the modes from the test and analysis are in agreement to within ±15%, which is considered an acceptable margin of error.

9
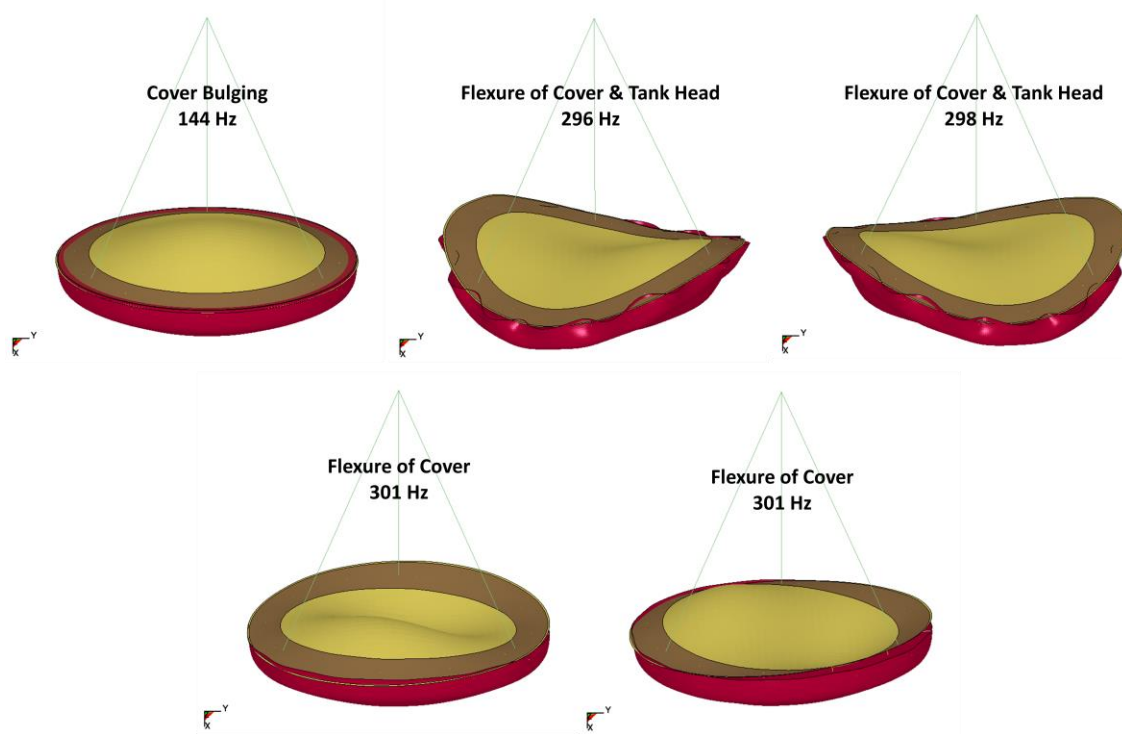
Figure 9. First Five Flexural Modes from Modal Analysis

Table 3. Comparison of Test and Analysis Vibration Modes

Mode	Test Mode Frequency (Hz)	Analysis Mode Frequency (Hz)	Error (%)
Bulging of Cover Plate	168	144	-14
Flexure of Cover Plate and Tank Head	259	296	14
Flexure of Cover Plate and Tank Head	259	298	15
Flexure of Cover Plate	310	301	-3
Flexure of Cover Plate	310	301	-3

5. Approach for Comparing Test and Simulation Data

5.1. Processing of Test Data

For each test, the raw data record typically begins approximately 5 seconds before release of the drop hook, and extends approximately 20 seconds after release. The sampling rate was 40,000 Hz, which yielded data files for each sensor with approximately a million

10

points. To make the data more manageable, the time histories were snipped to 10,000 points around the time of impact. The pressure peak at Pressure Gage 7 was used as a marker. The snipped data record began 1000 steps (0.025 seconds) prior to the Pressure Gage 7 peak, and extended 9000 steps (0.225) seconds after the peak.

5.2. Acceleration

For comparing test and simulation acceleration histories, a 600 Hz Butterworth filter was used. This is a relatively high filter frequency and admits a significant amount of noise. In Figure 10, acceleration histories for 8/30 Drop 3 (2-feet) are shown that have been filtered at a various frequencies. Note that the vertical scale (acceleration) is varied on each graph based on the amplitude. A filter frequency of 600 Hz was chosen because it is well above the first vibration modes of the tank head.
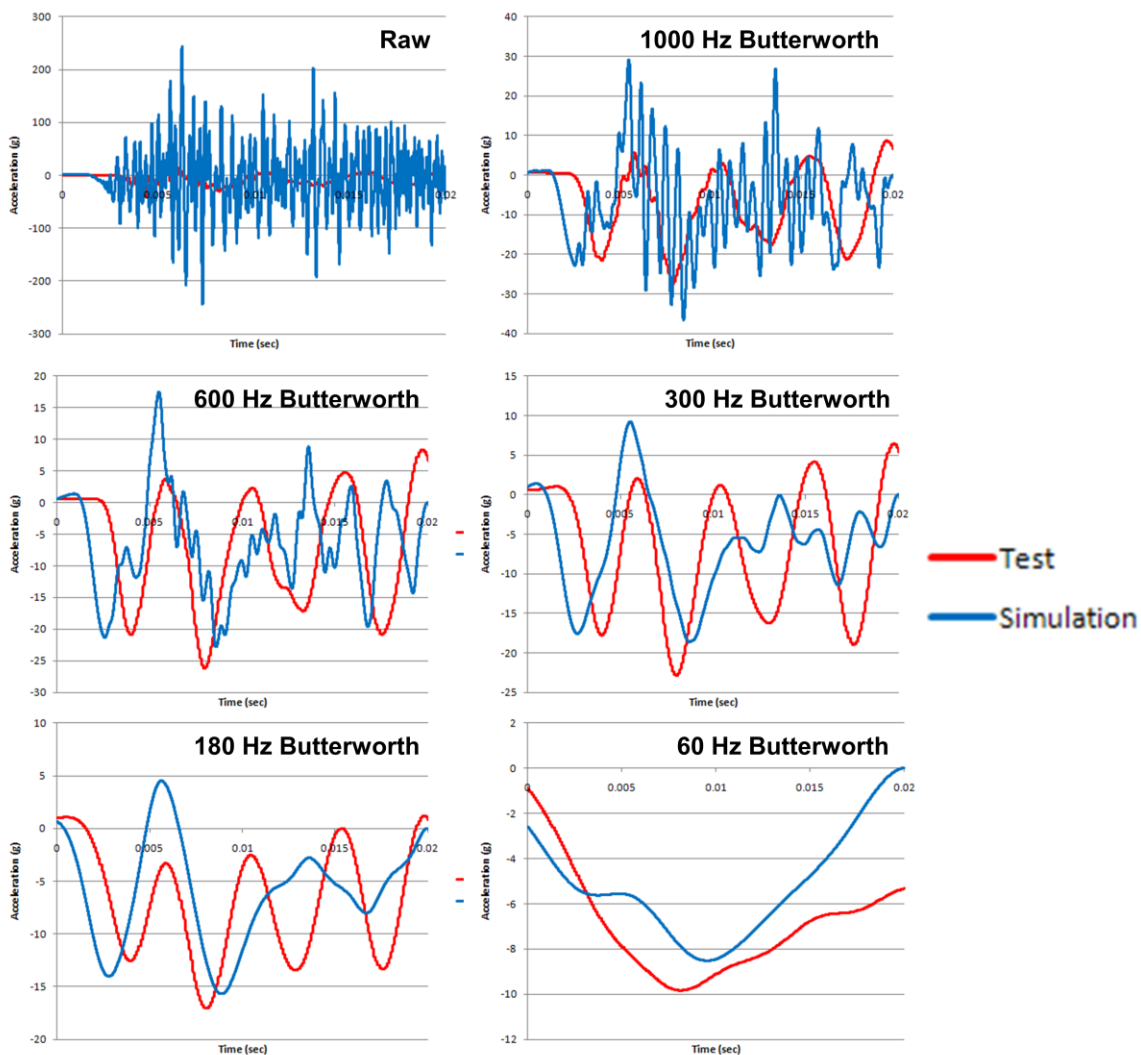
Figure 10. Acceleration History Filter Frequency Comparison

11

When comparing test and simulation acceleration histories, no formal method was used to synchronize the acceleration histories. The initial peaks were approximately aligned based on visual inspection.

5.3. Pressure

The test and simulation pressure histories were aligned by matching the times of the initial peak at Pressure Gage 9. This is illustrated for 8/30 Drop 3 (2-feet) in Figure 11.
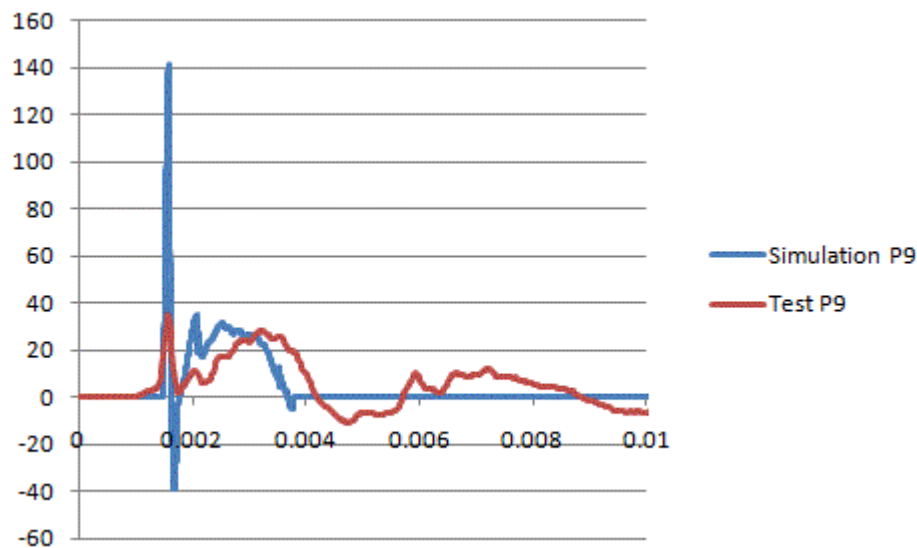
Figure 11. Matching Timing of Initial Spike at Pressure Gage 9

The diameter of the pressure transducers was approximately one-eighth inch. In the LS-DYNA model, pressure histories were output for surface segments that corresponded to individual shell elements of the tank head. The edge length of a typical element of the tank head was approximately 0.2 inches. The duration of the initial pressure pulse was so short that the difference in the area over which it was measured could affect the measurement. No attempt was made to compensate for this in the test versus simulation comparisons. The areas over which the pressure was measured were not vastly different. Theoretically, the test should produce the higher measurement since it was over a smaller area, and should better capture the peak of the passing pressure wave; however, the simulations generally produced the higher peaks.

Impulse was calculated for the simulation time histories by integrating the pressure histories. The impulse calculation was not performed with the test data due to difficulty in obtaining a reliable result. For the test data, the calculated impulse was highly sensitive to the time period over which the integration was performed, and drift in the zeroing of the pressure history could result in a large change in the result.

5.4. Deflection

In the tests, the relative deflection between the cover plate and the tank head was recorded at three locations using string pots. Deflection histories for the simulations were determined by subtracting the displacements at the cover plate from displacements at the tank head. As with the pressure histories, the deflection histories were synchronized based on the timing of the peak pressure at Pressure Gage 9.

The deflection histories from the tests were smoothed by computing a 0.25 millisecond running average, which reduced high frequency noise. The time averaging was done only to make it easier to distinguish the individual curves. Figure 12 illustrates the difference between the raw and time-averaged deflection histories. Time averaging was used only for the test deflection histories, not for the simulation deflection histories.
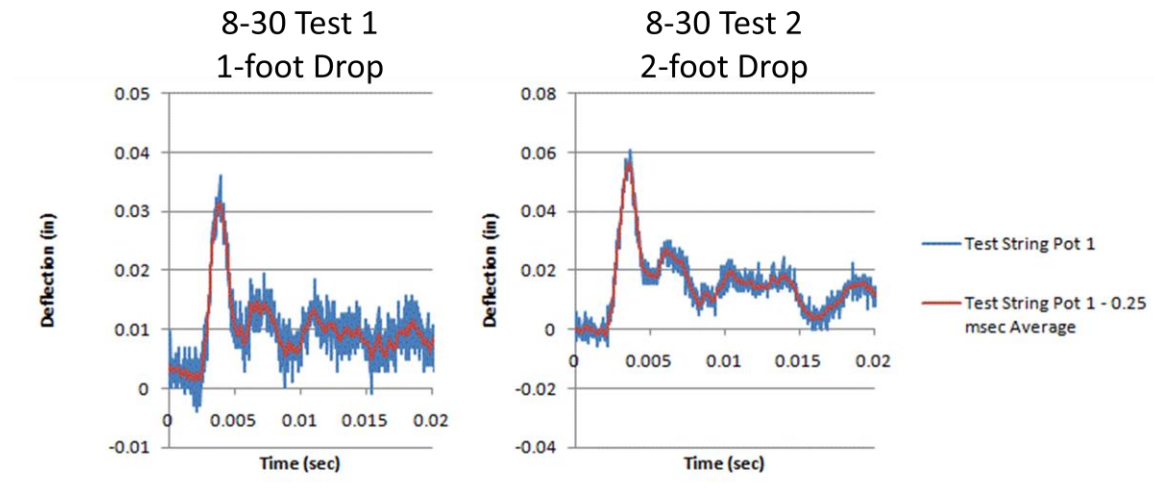
Figure 12. Raw and 0.25-millisecond Time Averaged Deflection Histories

5.5. Stress

The test article featured four rectangular strain gage rosettes. Each rosette consisted of three strain gages: A, B, and C. Strain Gages A and C were at right angles to one another. Strain Gage B was rotated forty-five degrees relative to A and C. The strain data from the rosettes was used to compute von Mises stresses. The equations are provided in Figure 13.

13

Rectangular Strain Gage Rosette

Gage A

Gage B

X

Gage C

Y
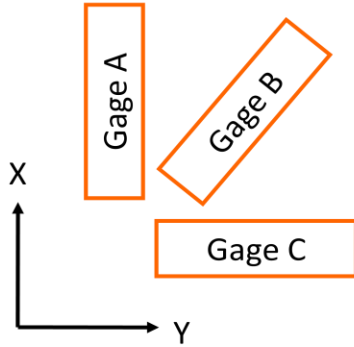
Measured Strains:

ε_A, ε_B, ε_C

Resolve to X,Y System:

$\varepsilon_X = \varepsilon_A$

$\varepsilon_Y = \varepsilon_C$

$\gamma_{XY} = 2 * \varepsilon_B - (\varepsilon_A + \varepsilon_C)$

Use Mohr's Circle to Determine Principal Strains:

$\gamma_{MAX} = 2 * \sqrt{(\gamma_{XY}/2)^2 + ((\varepsilon_X - \varepsilon_Y)/2)^2}$

$\varepsilon_1 = (\varepsilon_X + \varepsilon_Y)/2 + \gamma_{MAX}/2$

$\varepsilon_2 = (\varepsilon_X + \varepsilon_Y)/2 - \gamma_{MAX}/2$

Calculate Principal Stresses:

$\sigma_1 = E/(1 - \nu^2)*(\varepsilon_1 + \nu * \varepsilon_2)$

$\sigma_2 = E/(1 - \nu^2)*(\varepsilon_2 + \nu * \varepsilon_1)$

$\tau_{MAX} = G * \gamma_{MAX}$

Calculate Von Mises Stress:

$\sigma_{VM} = 1/\sqrt{2} * \sqrt{(\sigma_1^2 + \sigma_2^2 + (\sigma_1 - \sigma_2)^2}$

Figure 13. Von Mises Stress Calculation for Strain Gage Data

The strain gage data was rezeroed by subtracting the average of the first 800 steps of the snipped data record. This was the average over 0.02 seconds starting 0.025 seconds before the peak at Pressure Gage 7. As with the pressure histories, the test and simulation stress histories were synchronized based on the timing of the peak pressure at Pressure Gage 9.

Plots were made of the plastic strain from the simulations. There was no means to directly correlate this with test data. Surface scans before and after the test series were used to generate a contour map of the change in geometry of the tank head. This verified that plastic strain had occurred, but did not provide information on the actual magnitude of the plastic strain at a given location due to any single test.

6. Sensitivity Studies

6.1. Sensitivity to Coupling Stiffness

The baseline coupling stiffness was designated Curve 11 and featured a pressure of 200

psi at a penetration distance of 0.02 inches. Simulations were performed of one-foot and two-foot drops using variants of the baseline curve that were $1/100^{th}$ as stiff, $1/10^{th}$ as stiff, and 10 times as stiff. All other parameters reflected the baseline model, including a fluid element size of approximately 0.2 inches, and 50% critical damping of the coupling surface.

Figure 14 illustrates acceleration histories for the coupling stiffness variants. The acceleration responses measured in 8-30 Test 1 (1-foot drop) and 8-30 Test 2 (2-foot drop) are also shown. The simulation acceleration histories overlay very closely except for the lowest coupling stiffness, Curve 11 x 0.01. The conclusion is that the acceleration histories are not highly sensitive to coupling stiffness provided that the coupling stiffness is adequately high.
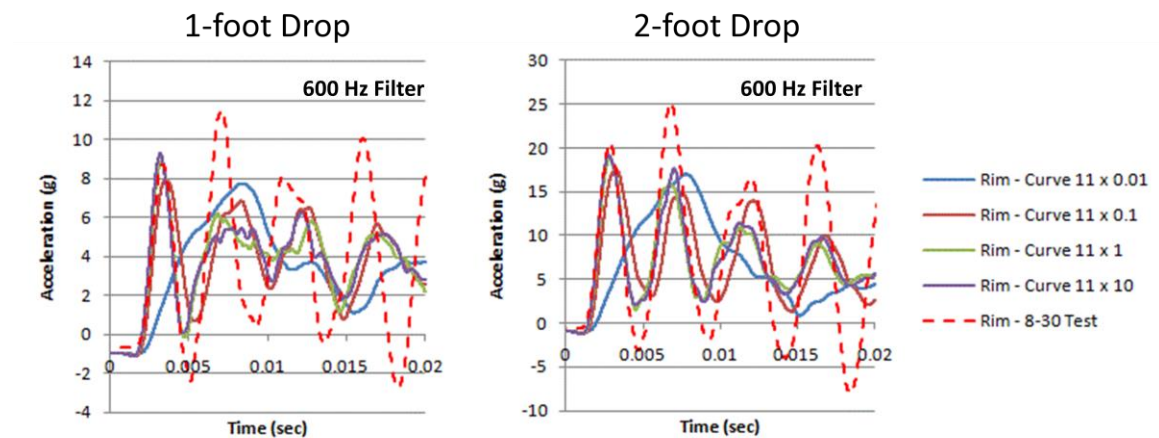
Figure 14. Acceleration Histories for Coupling Stiffness Variants

Figure 15 illustrates the histories at Pressure Gage 7 for the coupling stiffness variants. All of the pressure histories show initial peaks that are substantially different. The higher stiffness curves give similar predictions for the later-time pressure response. The conclusion is that the pressure history peaks are extremely sensitive to coupling stiffness.

15
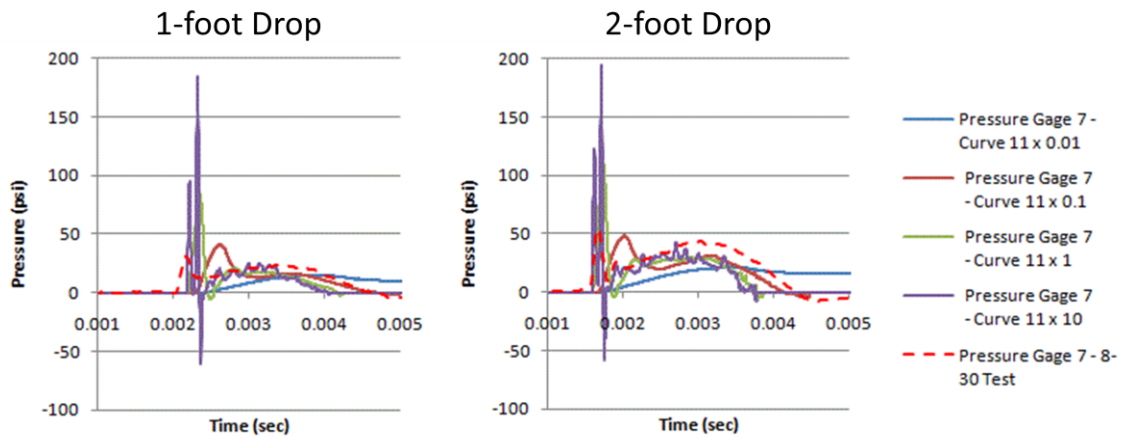
Figure 15. Gage 7 Pressure Histories for Coupling Stiffness Variants

Figure 16 illustrates pressure contours 0.003 seconds after impact for the coupling stiffness variants. The pressure contours should show a "Coliseum Effect" [6] pressure distribution with a tight ring of high pressure at the perimeter of the contact patch. The coupling stiffness variants show this to varying degrees, except for the lowest coupling stiffness, Curve 11 x 0.01. The pressure contours that most closely reflect the expected distribution are for Curve 11 x 1.
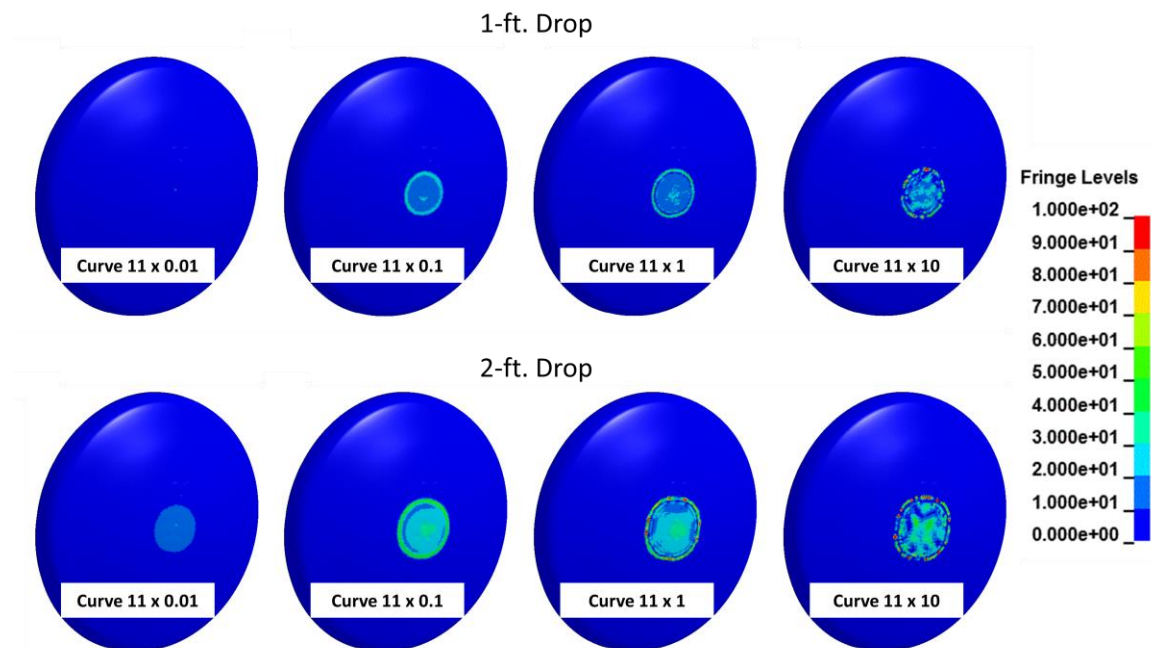
Figure 16. Pressure Contours 0.003 seconds after Impact for Coupling Stiffness Variants

16

Figure 17 shows the impulse at each of the pressure gage locations for each of the coupling stiffness variants. The impulse is calculated as the time integration of the pressure pulse. The results show substantial variation in the impulse; however, the variation is much less than the factor of ten differences in the coupling stiffnesses. There is no clear trend of higher coupling stiffnesses resulting in either higher or lower impulses.
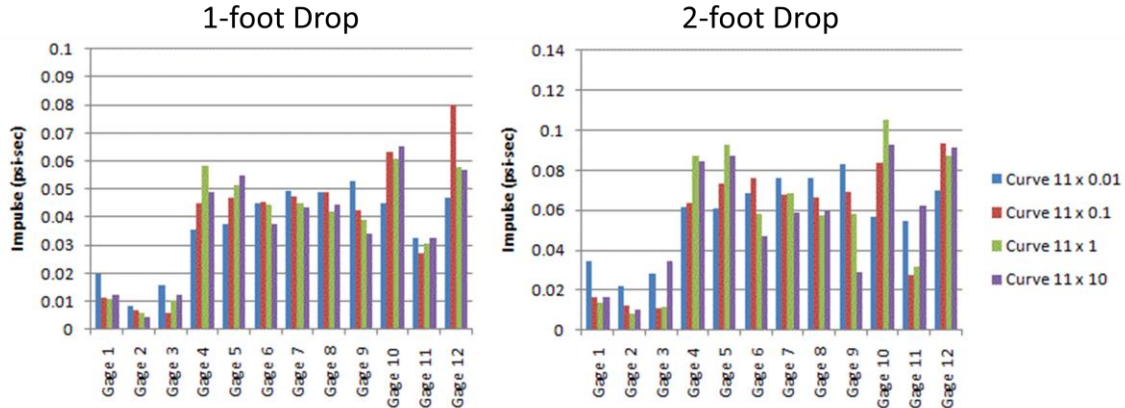
Figure 17. Impulse for Coupling Stiffness Variants

Figure 18 shows the relative deflection between the cover plate and the tank head at String Pot 2. The deflection histories overlay closely, except for the lowest coupling stiffness, Curve 11 x 0.01. The conclusion is that deflections are not highly sensitive to coupling stiffness.
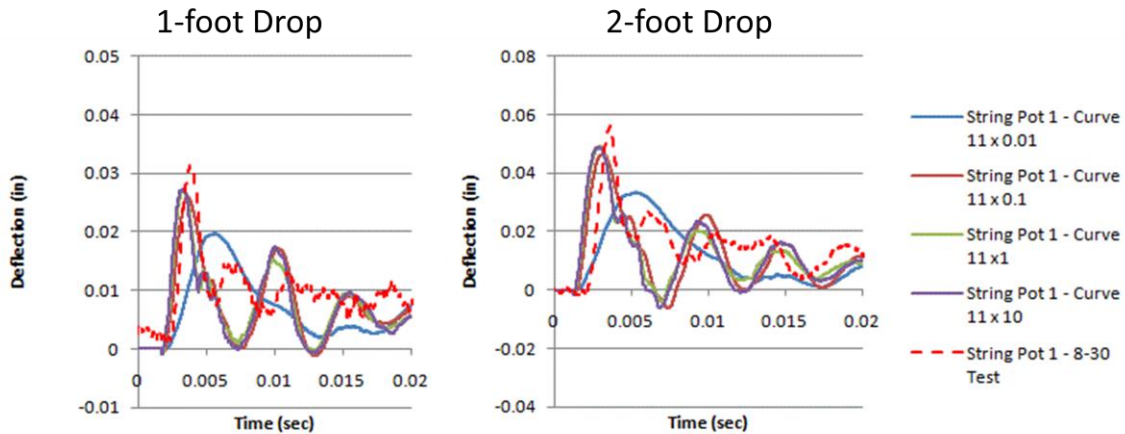
Figure 18. String Pot 1 Deflection Histories for Coupling Stiffness Variants

The histories of the von Mises stresses at Strain Gage 2 are illustrated in Figure 19. The curves overlay closely, except for the lowest coupling stiffness variant, Curve 11 x 0.01. The conclusion is that the stress histories are not highly sensitive to coupling stiffness.

17
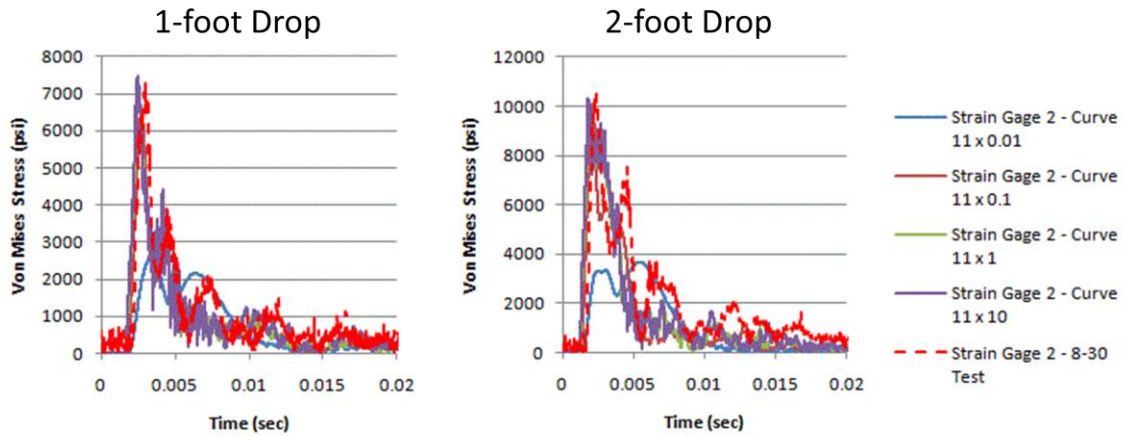
Figure 19. Strain Gage 2 Von Mises Stress Histories for Coupling Stiffness Variants

The simulations for the 1-foot drops predicted no plastic strain. The simulations for the 2-foot drops predicted a small region of plastic strain at the outer surface of the tank head at the apex. Contours of the plastic strain at the conclusions of the simulations are shown in Figure 20. The variants with the lowest coupling stiffness, Curve 11 x 0.0 and Curve 11 x 0.1, barely show any plastic strain. The other variants show similar patches of plastic strain at the apex.
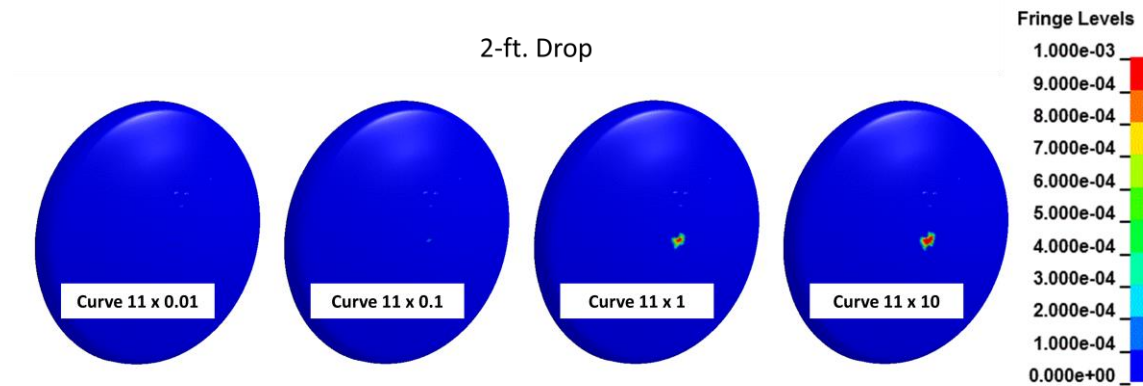
Figure 20. Plastic Strain Contours for Coupling Stiffness Variants of Simulations of 2-foot Drops

Figure 21 shows the penetration of the fluid through the coupling interface at 0.003 seconds after impact. The lowest coupling stiffnesses, Curve 11 x 0.01 and Curve 11 x 0.1, show nearly continuous penetration across the contact patch. The other coupling stiffnesses produce substantially less penetration. It should be noted that penetration is different from leakage. Penetration must occur in order for the coupling algorithm to generate a coupling pressure. Fluid that penetrates the structural boundary continues to be resisted by the coupling pressure. Leakage refers to fluid that has escaped across the coupling surface, and is no longer resisted by the coupling pressure.

18

1-ft. Drop

2-ft. Drop
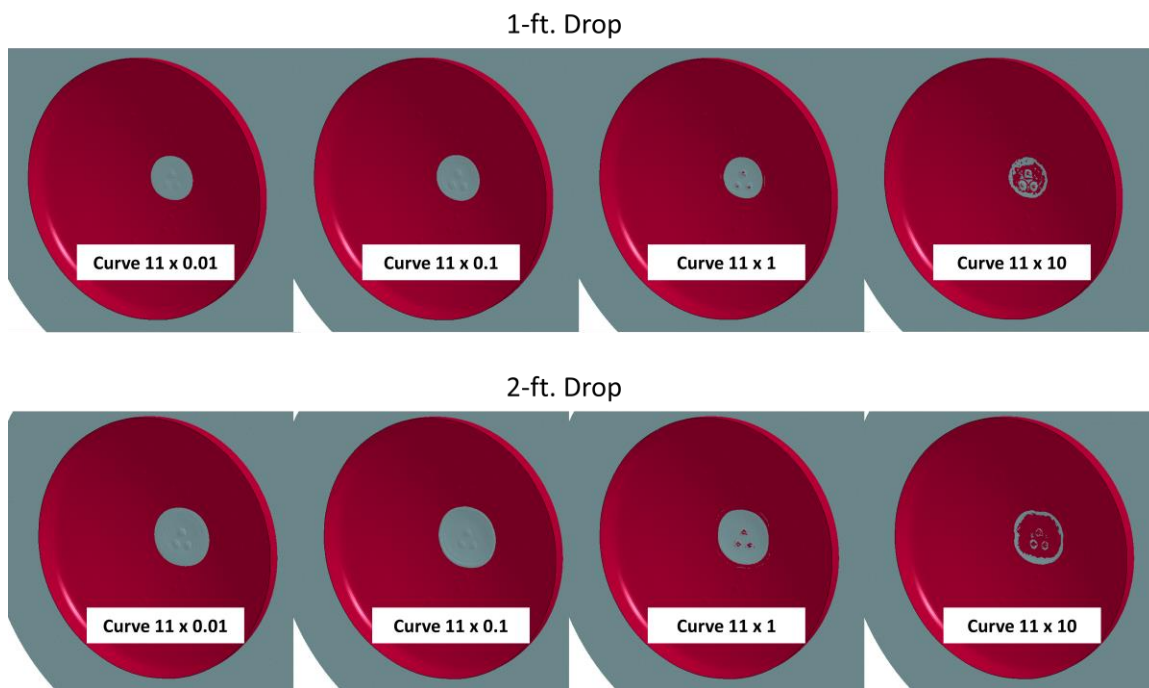
Figure 21. Fluid Penetration through Coupling Interface 0.003 seconds after Impact for Coupling Stiffness Variants

Based on these results, it was concluded that the baseline coupling stiffness, Curve 11 x 1, produced the most credible simulation results. As a consequence, the Curve 11 x 1 coupling stiffness was chosen for further comparisons with test data.

6.2. Sensitivity to Coupling Surface Damping

The baseline model featured 50% critical damping of the coupling surface, which was invoked by setting the parameter DAMP equal to 0.50. The LS-DYNA documentation offers only a minimal description of the DAMP parameter. It is understood that it places a damper in parallel to the fluid-structure coupling stiffness, and that the damping coefficient is set to a percentage of critical damping based on the stiffness of the coupling spring and the masses of the nodes at either end of the spring. Damping is typically used to remove energy from an oscillatory system. Ideally, the coupling pressure history should appear as one major spike with no oscillation, so a high percentage of critical damping is considered suitable. The damper could be considered as a secondary means of transmitting the contact force based on penetration velocity rather than penetration distance.

Simulations were performed of one-foot and two-foot drops with 0%, 20%, 50%, and 80% critical damping. All other parameters reflected the baseline model, including a fluid element size of approximately 0.2 inches and the Curve 11 x 1 coupling stiffness.

Figure 22 illustrates acceleration histories for the damping variants. The acceleration responses measured in 8-30 Test 1 (1-foot drop) and 8-30 Test 2 (2-foot drop) are also shown. The curves overlay very closely. The conclusion is that the acceleration histories are not highly sensitive to coupling surface damping.
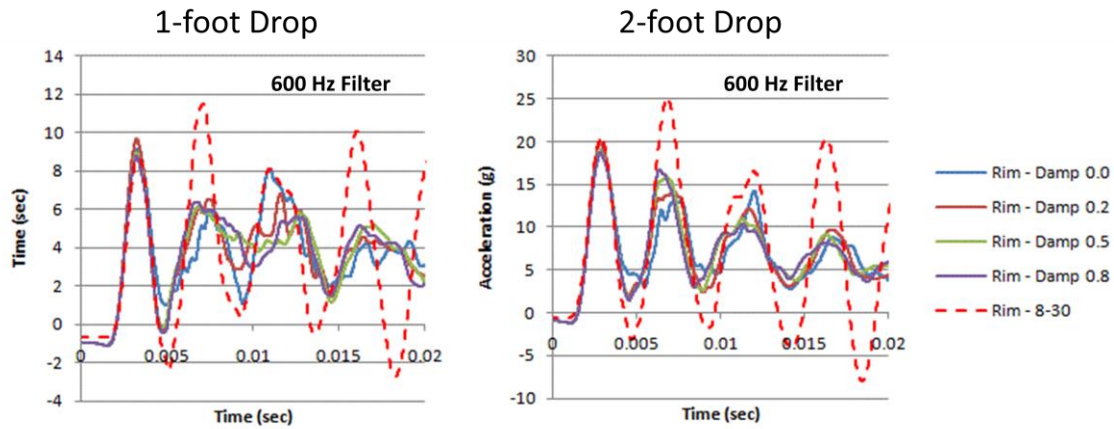
Figure 22. Acceleration Histories for Damping Variants

Figure 23 illustrates the pressure histories at Gage 7 for the damping variants. The variant without damping shows a succession of isolated pressure spikes. This is consistent with a series of rings of high pressure seen in some simulations. This is very unlike the expected coliseum effect response with a single ring of high pressure encircling a broad region of relatively low pressure. All the curves over-predict the initial pressure peak. The initial pressure peak is not highly sensitive to damping, but higher levels of damping do result in negative overshoot following the initial peak. Based on this, an intermediate level of damping was the favored option.
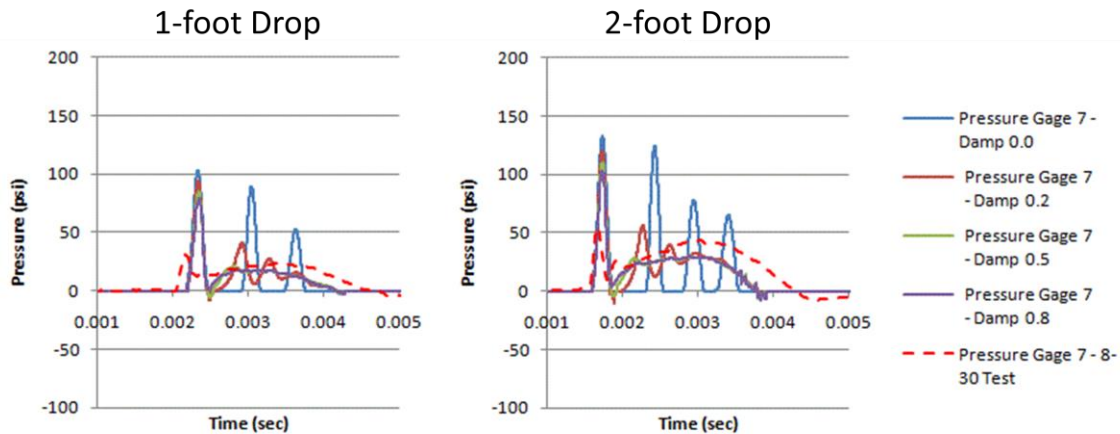
Figure 23. Gage 7 Pressure Histories for Damping Variants

20

Figure 24 illustrates pressure contours 0.003 seconds after impact for the damping variants. The variant with no damping shows a series of concentric rings of high pressure, which does not match the expected coliseum effect. The pressure contours show diminishing returns for damping increased beyond 50%.
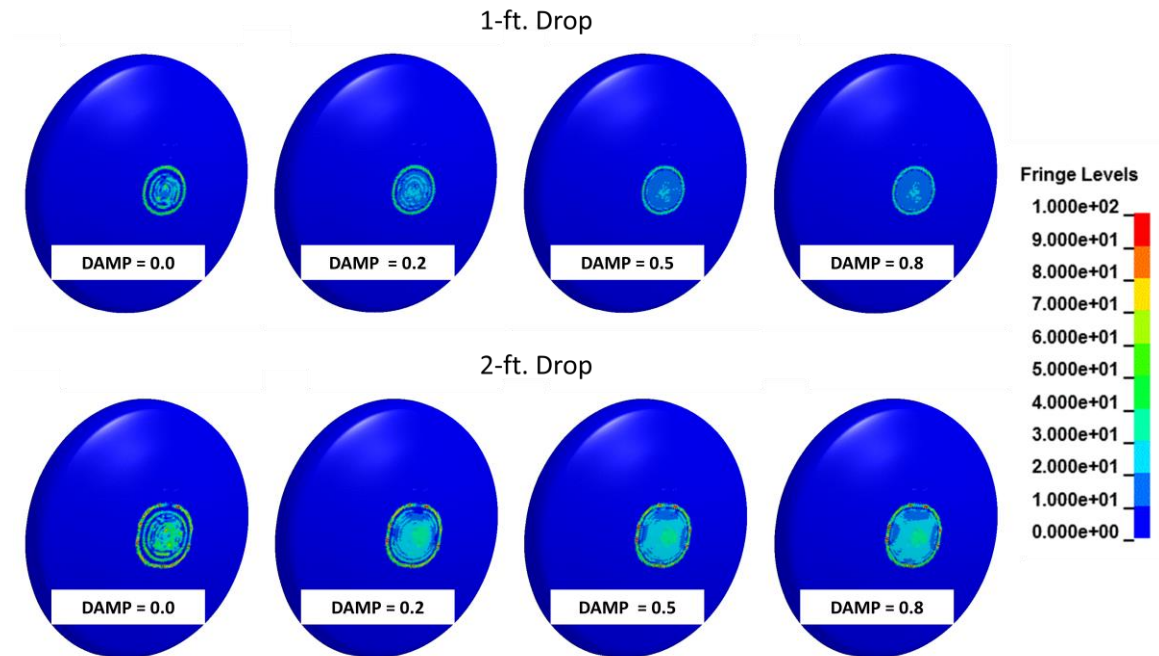
Figure 24. Pressure Contours 0.003 seconds after Impact for Damping Variants

Figure 25 shows the impulse at each of the pressure gage locations for each of the damping variants. There is no clear trend of higher damping resulting in either higher or lower impulses.
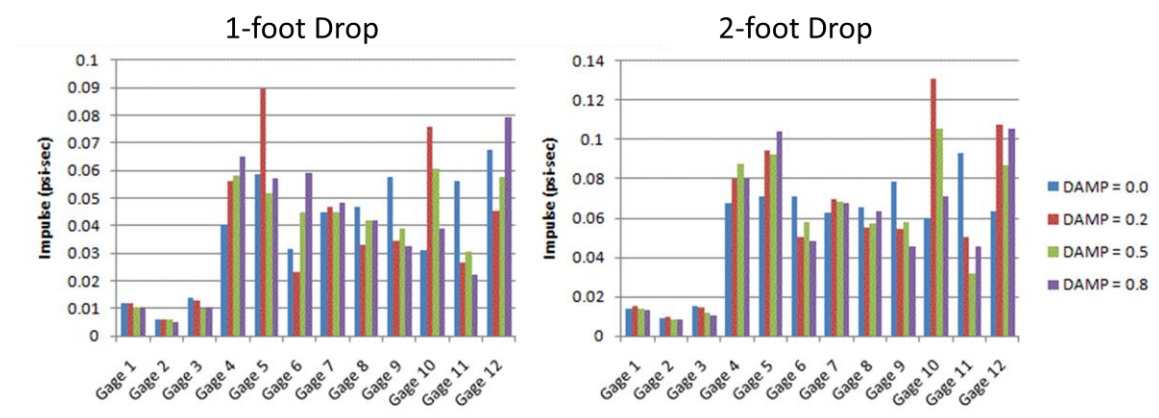
Figure 25. Impulse for Damping Variants

Figure 26 shows the relative deflection between the cover plate and the tank head at String Pot 1. The deflection histories overlay closely. The conclusion is that deflections are not highly sensitive to coupling surface damping.
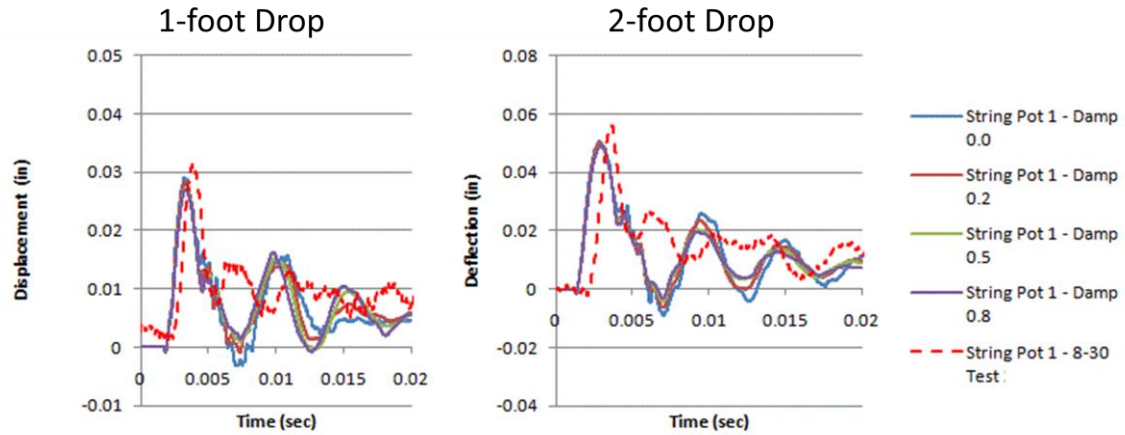
Figure 26. String Pot 1 Deflection Histories for Damping Variants

Von Mises stress histories at Strain Gage 2 are illustrated in Figure 27. The curves overlay closely. The conclusion is that the stress histories are not highly sensitive to coupling surface damping.
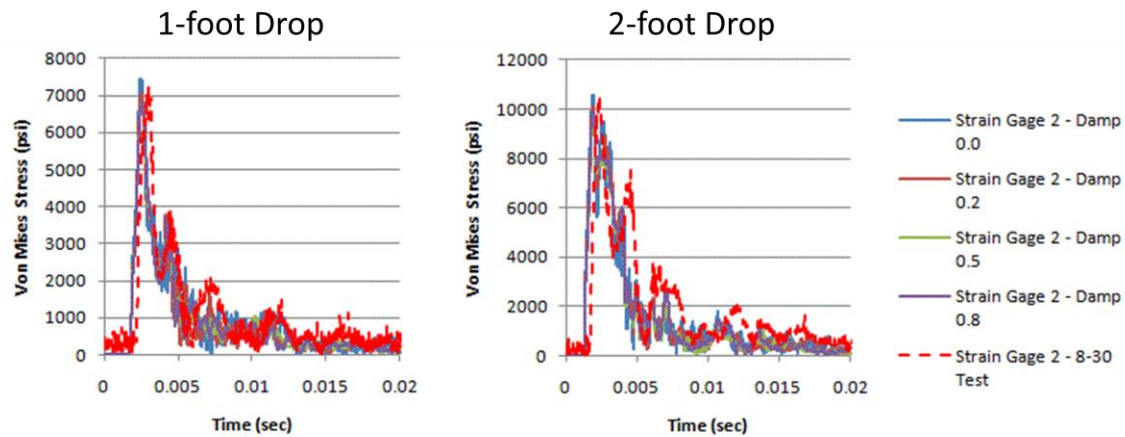
Figure 27. Strain Gage 2 Stress Histories for Damping Variants

The simulations for the 1-foot drops predicted no plastic strain. The simulations for the 2-foot drops predicted a small region of plastic strain at the outer surface of the tank head at the apex. Contours of the plastic strain at the conclusions of the simulations for the damping variants are shown in Figure 28. The results show that the plastic strain is

22

relatively insensitive to coupling surface damping.
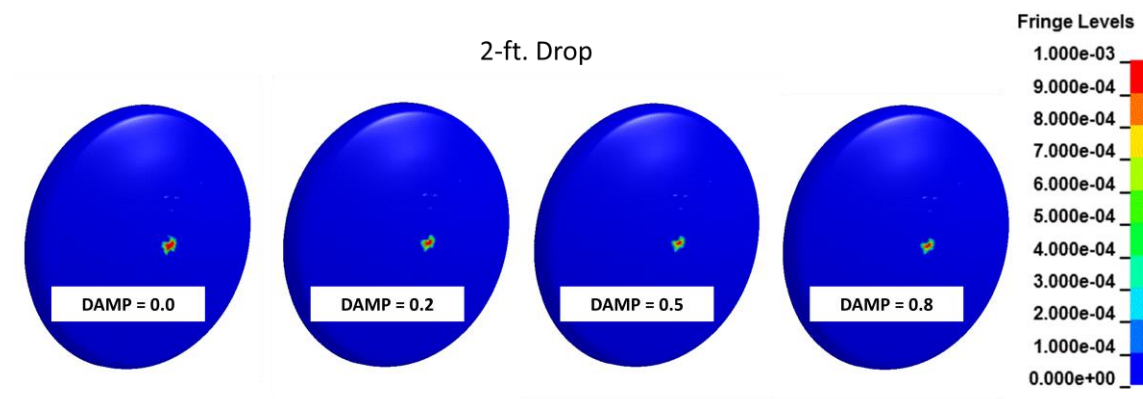
Figure 28. Plastic Strain Contours for Damping Variants of Simulations of 2-foot Drops

Figure 29 shows the penetration of the fluid through the coupling interface at 0.003 seconds after impact. The variant with no damping shows concentric rings of penetration. The other damping variants show penetration that is progressively more uniform across the region of contact.
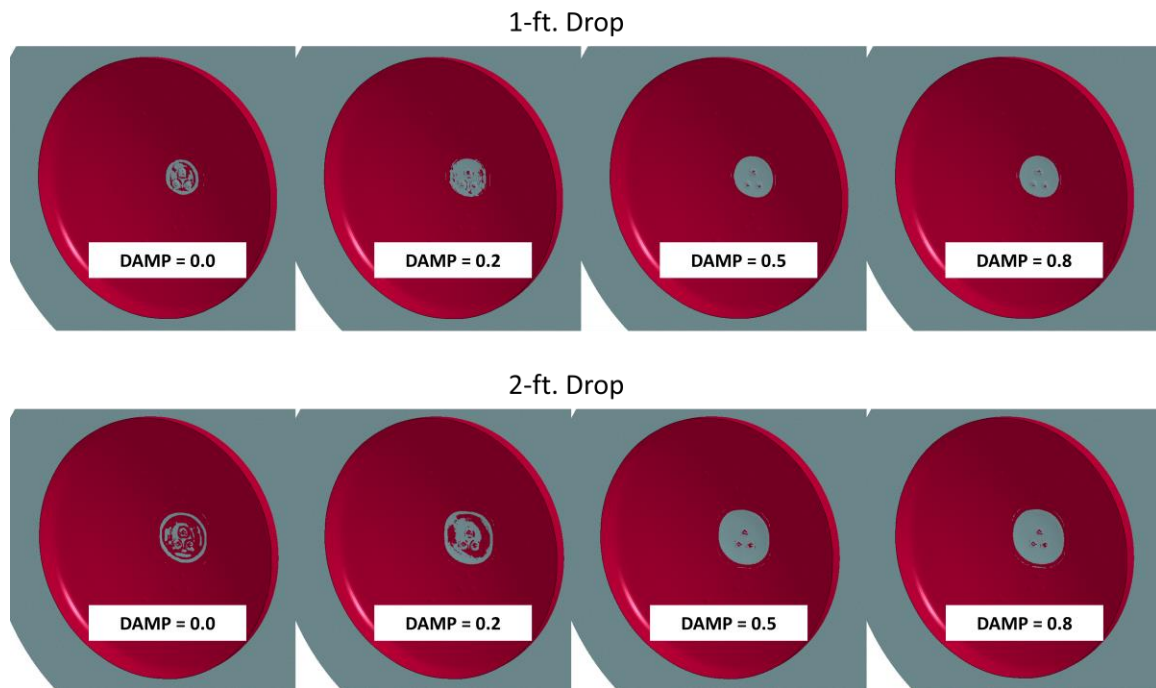
Figure 29. Fluid Penetration through Coupling Interface 0.003 seconds after Impact for Damping Variants

Based on these results, it was concluded that the baseline coupling surface damping of 50% produced a reasonable compromise between the elimination of multiple pressure

23

spikes and minimal negative overshoot following the initial pressure spike. As a consequence, 50% coupling surface damping was chosen for further comparisons with test data.

6.3. Sensitivity to Water Mesh Density

The baseline model featured a fluid element size of approximately 0.2 inches. Two variants were constructed with an element size of approximately 0.1 inches. The first variant, or small mesh, was created by scaling the baseline mesh by a one-half. The second variant, or refined mesh, was created by subdividing each element of the baseline fluid mesh into eight elements. The small mesh variant was actually smaller in diameter than the tank head, and was considered feasible only because the simulation is of such short duration that the tank head does not fully immerse. The simulation with the small mesh variant is of interest because it offers a means to provide a refined water mesh without incurring a large solution time penalty. The models are illustrated in Figure 30.

Baseline Mesh
Fluid Element Size = 0.2″
Outer Diameter = 60″
Depth = 21″

Refined Mesh
Fluid Element Size = 0.1″
Outer Diameter = 60″
Depth = 21″

Small Mesh
Fluid Element Size = 0.1″
Outer Diameter = 30″
Depth = 10.5″
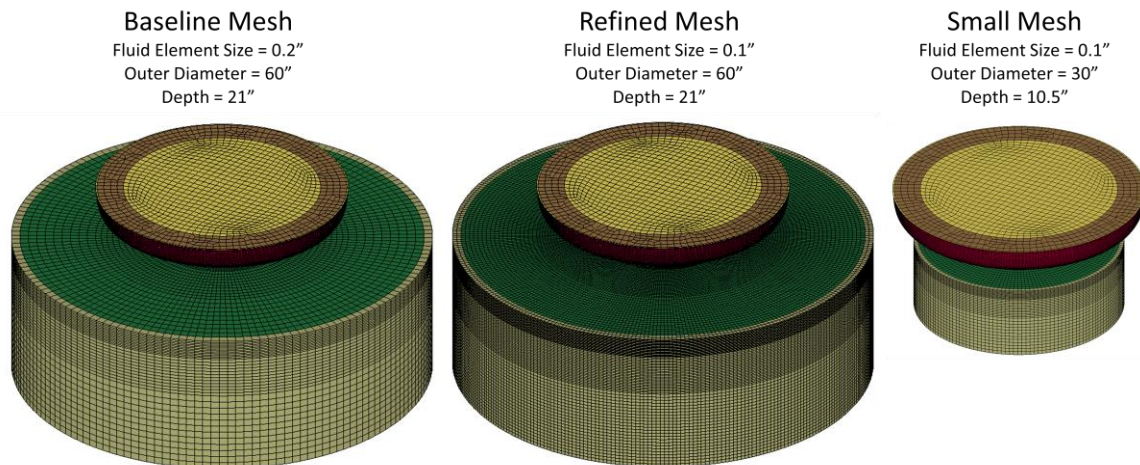
Figure 30. Water Mesh Density Variants

An additional variant was run with the minimum volume faction for fluid coupling, FRCMIN, set to 0.4, as opposed to the default value of 0.5. Reducing FRCMIN from the default value provides a means to tune the fluid-structure coupling. All other parameters reflect the baseline model, including Curve 11 x 1 coupling stiffness, and 50% critical damping at the coupling surface.

Figure 31 illustrates acceleration histories for the mesh density variants. The acceleration responses measured in 8-30 Test 1 (1-foot drop) and 8-30 Test 2 (2-foot drop) are also shown. The curves for the refined and small mesh variants show a much lower acceleration peak than the baseline mesh variants, and are in much poorer agreement with the initial peak accelerations from the tests. This is especially true for the two-foot drop.

The under-predictions of the initial acceleration peak for the finer meshes may be partly due to using the same coupling stiffness curve as the baseline mesh. The LS-DYNA Keyword User's Manual [5] suggests that the coupling stiffness curve be set to provide the peak expected pressure at a penetration distance equal to one-tenth the edge length of the fluid elements. This would suggest that a factor of two decrease in the fluid element should be accompanied by a factor of two increase in the coupling stiffness. This does not fully explain the results as the stiffness sensitivity comparison showed that a factor of ten change in the coupling stiffness was necessary to significantly change the response.
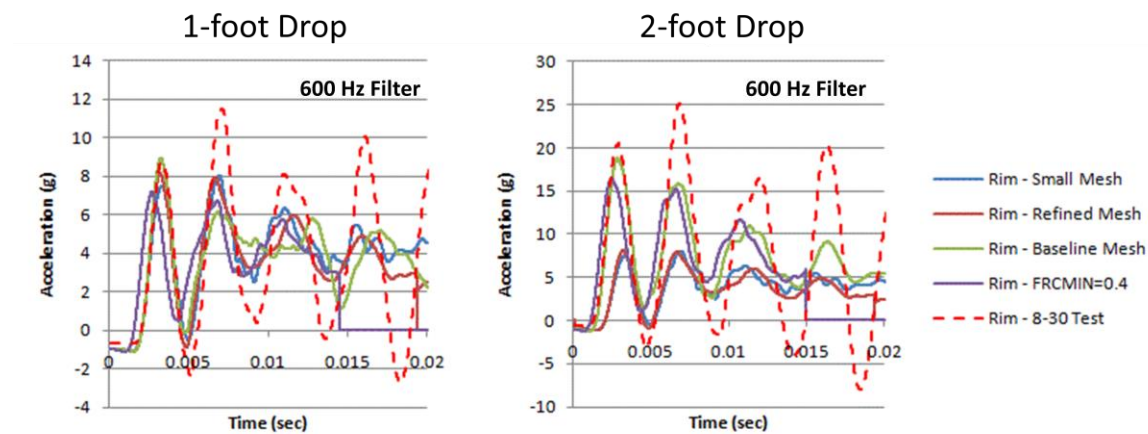
Figure 31. Acceleration Histories for Water Mesh Density Variants

Figure 32 illustrates the pressure histories at Gage 7 for the mesh density variants. The baseline mesh and the FRCMIN variant over-predicted the initial pressure peak. The refined and small meshes provided an initial peak pressure similar to the test data. The baseline mesh provided the best prediction of the later-time pressure response.
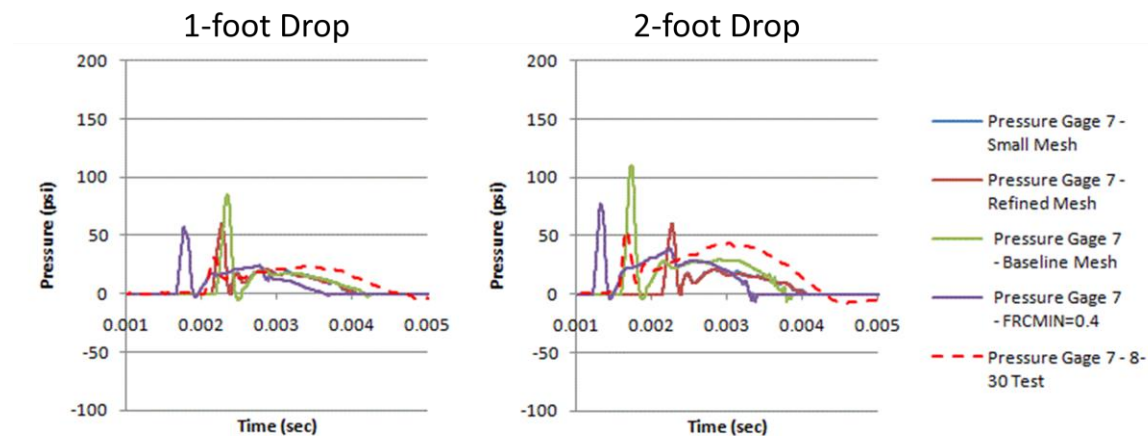
Figure 32. Gage 7 Pressure Histories for Water Mesh Density Variants

25

Figure 33 illustrates pressure contours 0.003 seconds after impact for the mesh density variants. All of the variants do a reasonable job of predicting a coliseum effect ring of high pressure at the perimeter of the contact patch that surrounds a region of much lower pressure.
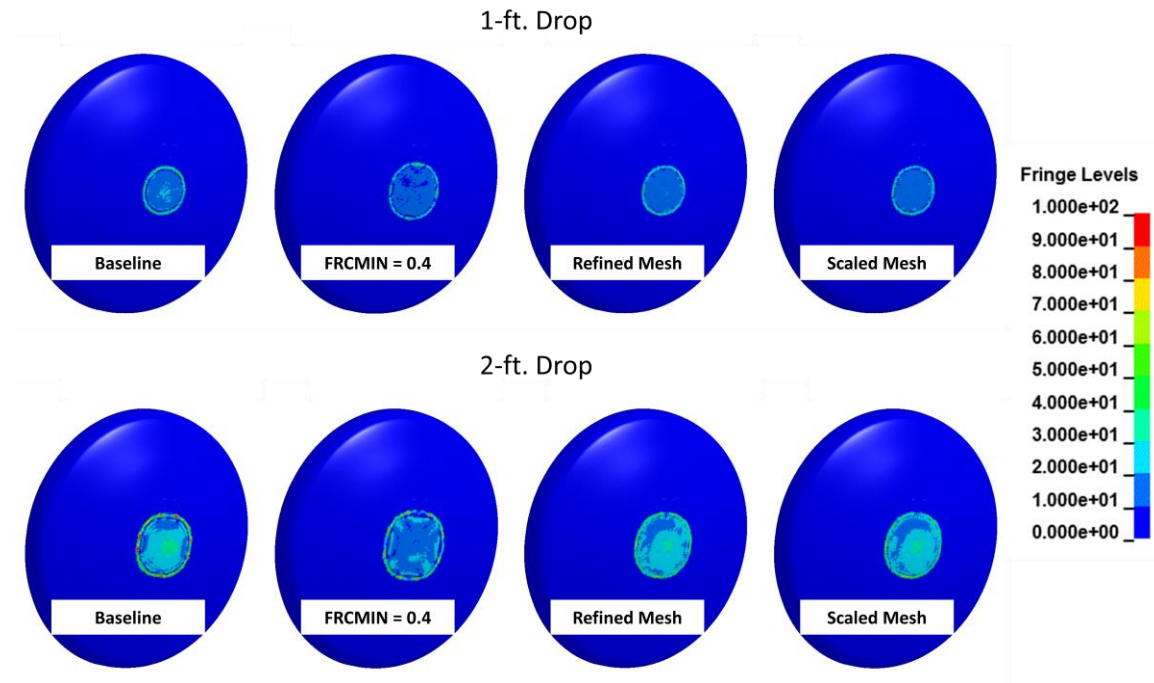
Figure 33. Pressure Contours 0.003 seconds after Impact for Water Mesh Density Variants

Figure 34 shows the impulse at each of the pressure gage locations for each of the mesh density variants. There is no clear trend of decreased water element size resulting in either higher or lower impulses.
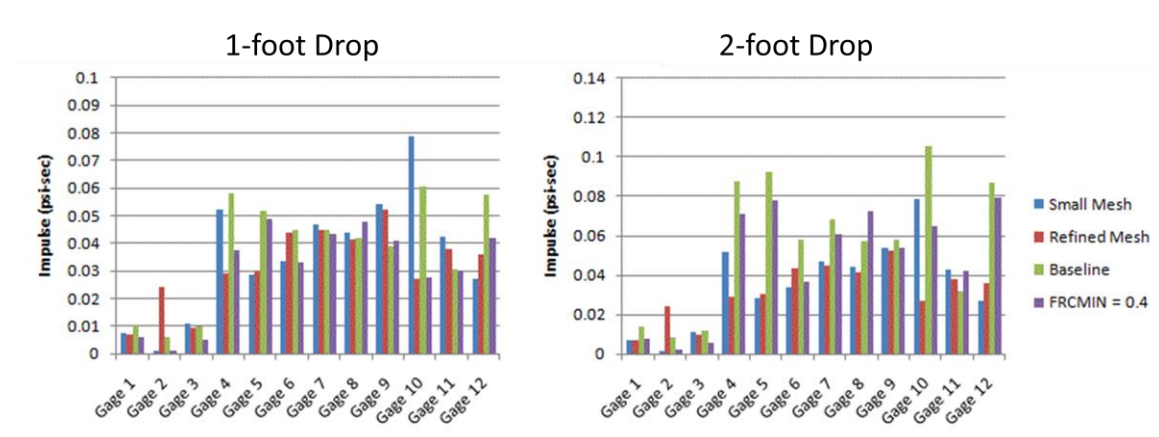
Figure 34. Impulse for Water Mesh Density Variants

26

Figure 35 shows the relative deflection between the cover plate and the tank head at String Pot 1. The time histories for the refined and small meshes are so similar that they are difficult to distinguish. The time histories from the refined and small meshes show substantially lower deflections, particularly for the two-foot drop, and do not compare as well with tests data as the baseline mesh and FRCMIN variant.
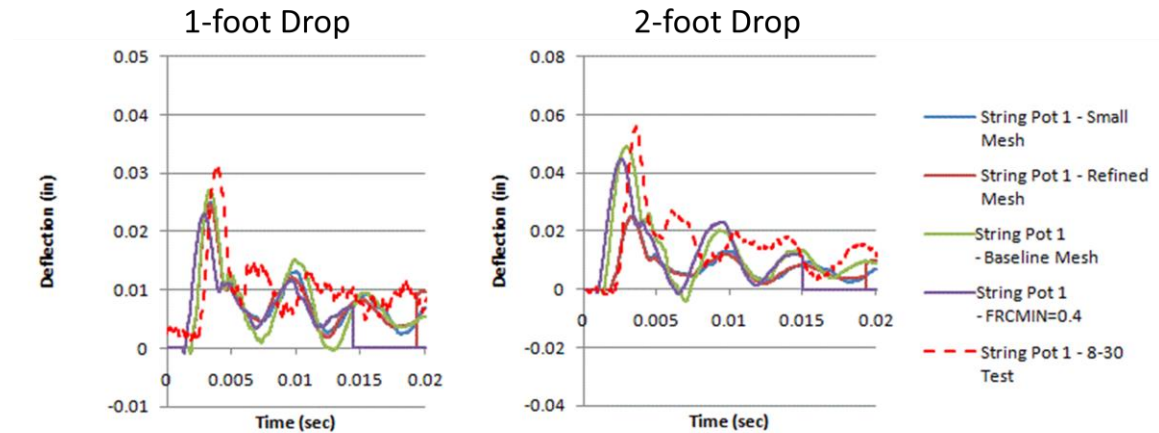
Figure 35. String Pot 1 Deflection Histories for Water Mesh Density Variants

The histories of the von Mises stresses at Strain Gage 2 are illustrated in Figure 36. The time histories for the refined and small meshes are again so similar that they are difficult to distinguish. The time histories from the refined and small meshes show substantially lower stresses, particularly for the two-foot drop, and do not compare as well with tests data as the baseline mesh and FRCMIN variant.
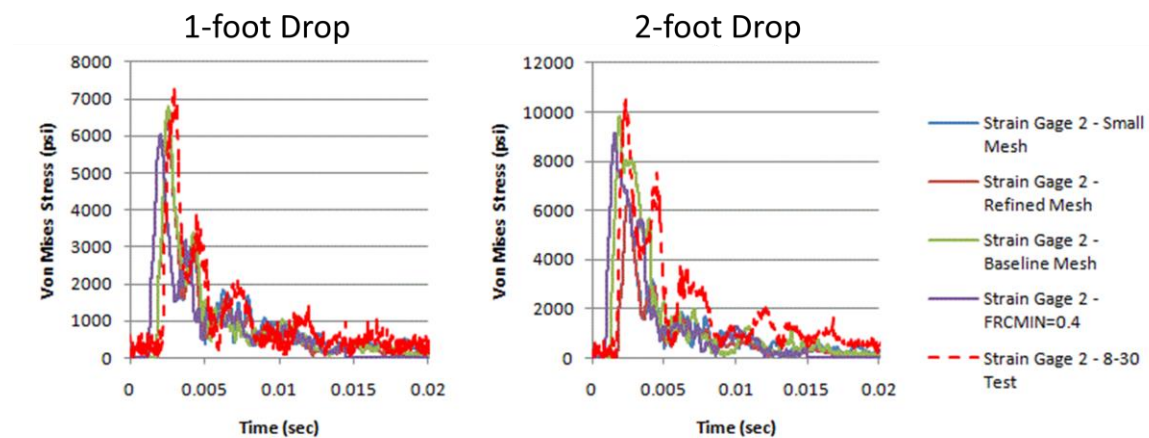
Figure 36. Strain Gage 2 Von Mises Stress Histories for Water Mesh Density Variants

The simulations for the 1-foot drops predicted no plastic strain. The simulations for the

2-foot drops predicted a small region of plastic strain at the outer surface of the tank head at the apex. Contours of the plastic strain at the conclusions of the simulations for the mesh density variants are shown in Figure 37. The refined and small mesh variants show smaller regions of plastic strain than the baseline simulation. The FRCMIN variant shows substantially less plastic strain than the other simulations.
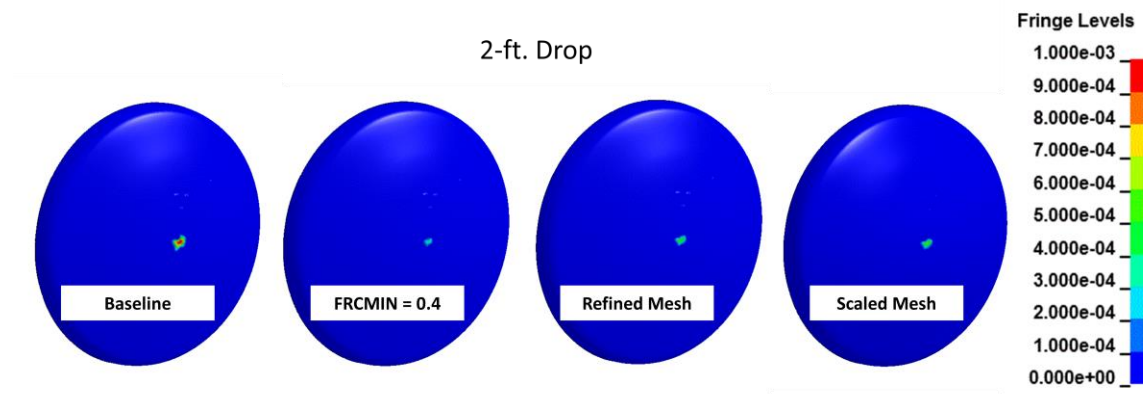
Figure 37. Plastic Strain Contours for Water Mesh Density Variants of Simulations of 2-foot Drops

Figure 38 shows the penetration of the fluid through the coupling interface at 0.003 seconds after impact. The refined and small mesh variants show less penetration than the baseline simulation. The FRCMIN variant shows no penetration. It has been observed that reducing FRCMIN from the default value of 0.5 results in the fluid anticipating the arrival of the test article. This represents no real world physical effect, and likely explains the apparent lack of penetration in the FRCMIN variant.
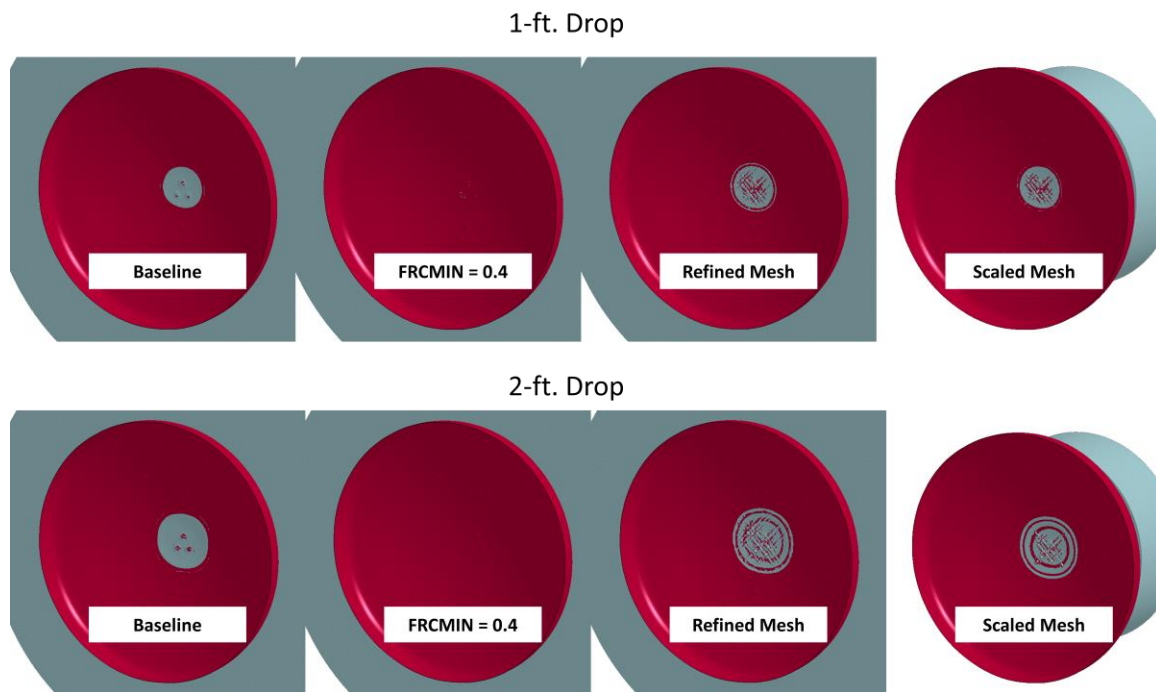
Figure 38. Fluid Penetration through Coupling Interface 0.003 seconds after Impact for Water Mesh Density Variants

The refined and small meshes produced the best predictions of the initial pressure peak, but otherwise did not perform as well as the baseline mesh. The finer meshes bring the disadvantage of requiring a longer solution time.

The minimum volume fraction for fluid coupling, FRCMIN, clearly does have an effect that could be useful in tuning the response of the model to better match a given set of test data; however, any such effect in tuning the model is completely artificial. There is no physics based rationale for choosing a value of FRCMIN other than the default, 0.5. One of the notable effects of reducing FRCMIN is that the water anticipates the arrival of the structure and begins moving in advance of the arrival of the structure. This has the consequences that the timing of the pressure peaks is moved forward and penetration of the water into the structure is reduced. Based on experiments with small test models, it was determined that FRCMIN moves the effective location of the free surface by an amount equal to $2*(0.5-FRCMIN)*d$, where d is the depth of the first layer of elements representing the air above the water. The free surface location correction is positive upward.

6.4. Sensitivity to Water Model

An issue of great interest is whether the parameters used for water landing simulations of full-scale spacecraft can be applied to the EWIT test simulations. In order to explore this,

three variants of the simulations have been run with progressive implementation of parameters based on other water landing simulations. The parameters for the water model variants are described in Table 4. The variants are illustrated in Figure 39.

Table 4. Water Model Variants

Parameter	Baseline	Variant 1	Variant 2	Variant 3
Water Element Size in way of Initial Impact	0.2 in.	0.25 in.	0.25 in.	0.25 in.
Water Depth	21 in.	26.25 in.	26.25 in.	8.64 in.
Air Height	3 in.	3.75 in.	3.75 in.	14.74 in.
Mesh Breadth	60 in.	75 in.	75 in.	81 in.
Coupling Stiffness (PFAC)	Curve 11	Curve 8 x 8	Curve 8 x 8	Curve 8 x 8
Coupling Damping (DAMP)	0.5	0.5	0.5	0.5
Number of Fluid Coupling Points (NQUAD)	2	2	2	2
Min. Vol. Fraction for Coupling (FRCMIN)	0.5	0.4	0.4	0.4
Solution Cycles per Mesh Advection (NADV)	1	1	5	5
Equation of State for Water	Linear Polynomial	Linear Polynomial	Gruneisen	Gruneisen
Equation of State for Air	Linear Polynomial	Linear Polynomial	Initial Void	Initial Void
Gravitational Preload	Mesh Preloaded	Mesh Preloaded	Instantaneous	Instantaneous
Reservoir Elements	Yes	Yes	No	No
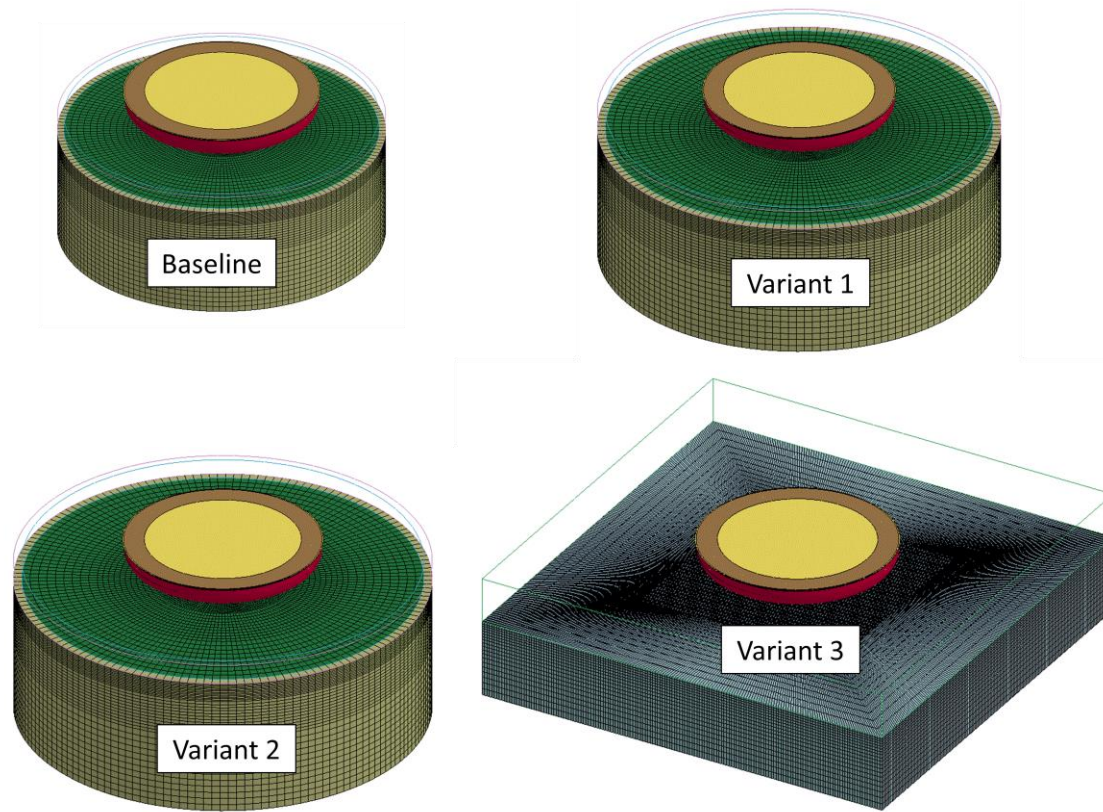
Figure 39. Water Model Variants

The coupling stiffness used for the baseline simulations, Curve 8, was scaled by a factor of eight. The LS-DYNA Keyword User's Manual [5] suggests that the coupling stiffness be based on a pressure equal to the peak anticipated pressure at a penetration distance equal to one-tenth the fluid element edge length, so the coupling stiffness is mesh specific. The scaled Curve 8 is compared to Curve 11 in Figure 40. Though Curve 11 gives higher coupling pressures than the scaled Curve 8, the terminal slopes are similar, 10,000 psi/inch for Curve 11 versus 11,814 psi/inch for the scaled Curve 8.
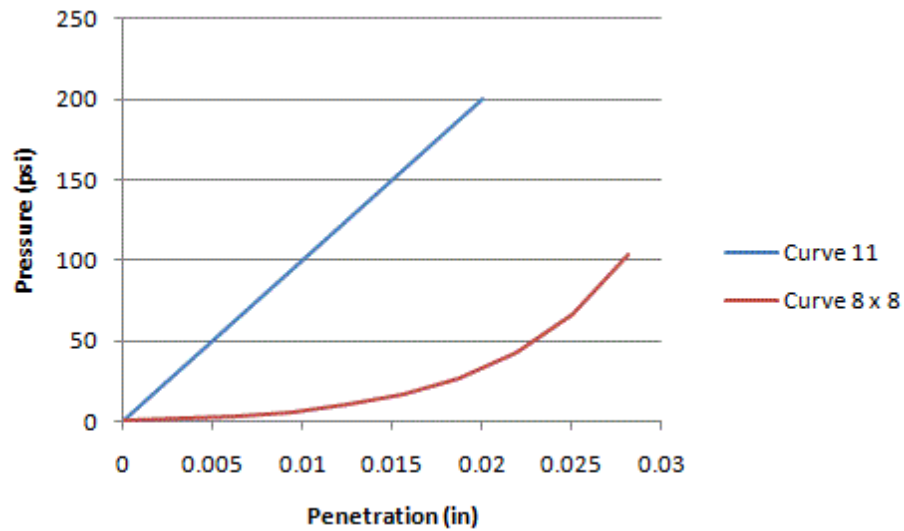
Figure 40. Coupling Stiffness Curves

Figure 41 illustrates acceleration histories for the water model variants. The acceleration responses measured in 8-30 Test 1 (1-foot drop) and 8-30 Test 2 (2-foot drop) are also shown. The baseline water model shows the highest acceleration for the initial peak and best agrees with test data.
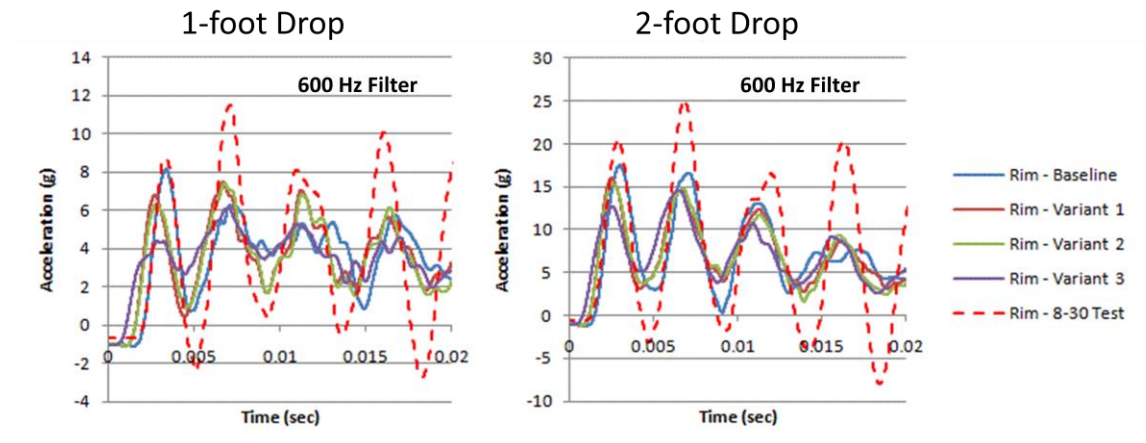
Figure 41. Acceleration Histories for Water Model Variants

Figure 42 illustrates the pressure histories at Gage 7 for the water model variants. All of the water model variants over-predicted the initial pressure peak. All provided reasonable predictions for the later-time pressure response.

32
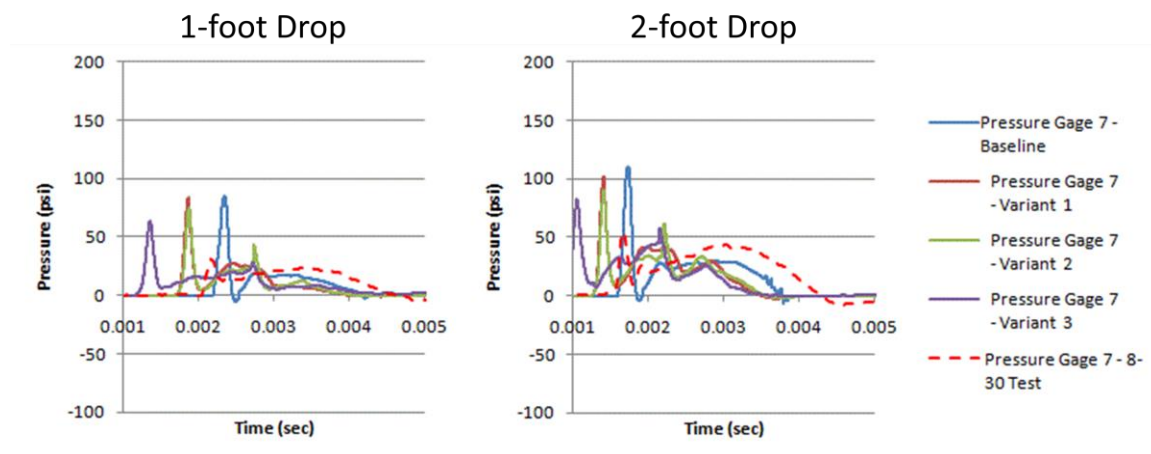
Figure 42. Gage 7 Pressure Histories for Water Model Variants

Figure 43 illustrates pressure contours 0.003 seconds after impact for the water model variants. The baseline water model provided the best approximation of a coliseum effect pressure pattern, with a narrow ring of high pressure at the perimeter of the contact patch, surrounding a region of lower pressure.
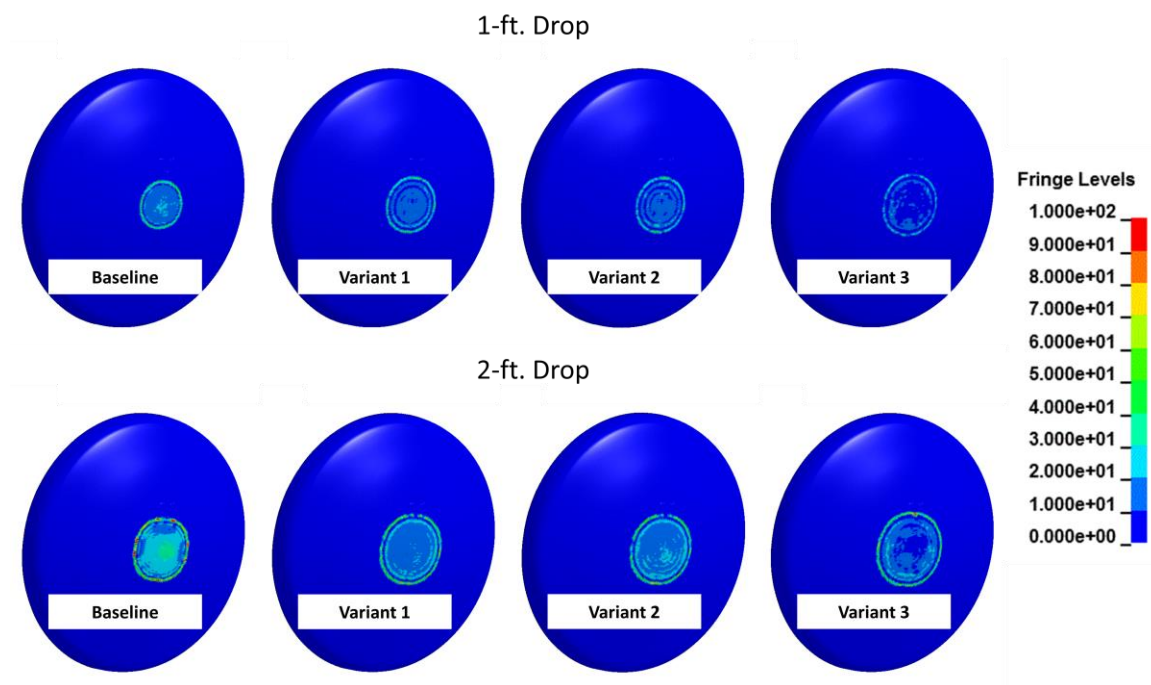
Figure 43. Pressure Contours 0.003 seconds after Impact for Water Model Variants

Figure 44 shows the impulse at each of the pressure gage locations for each of the water model variants. There is no clear trend for any particular water model resulting in either

higher or lower impulses.
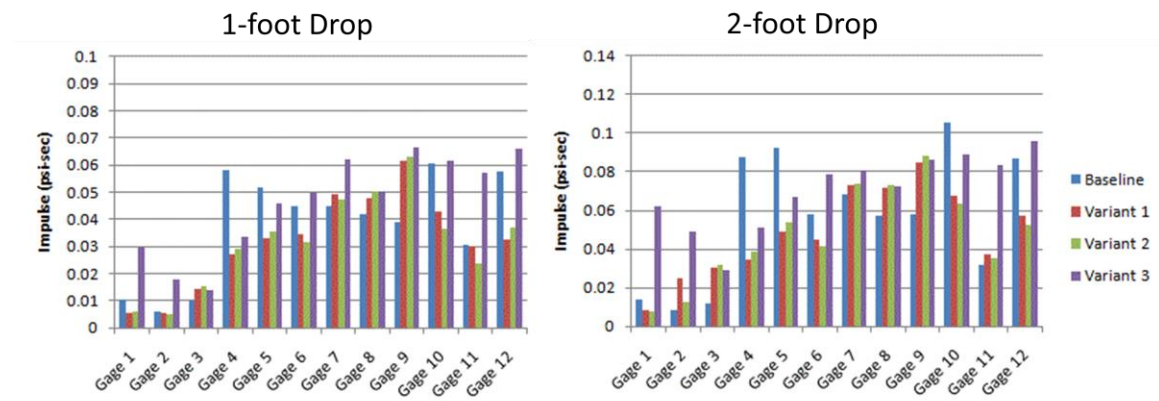
Figure 44. Impulse for Water Model Variants

Figure 45 shows the relative deflection between the cover plate and the tank head at String Pot 1. The baseline water model produced the highest initial peak, and best matched the test data.
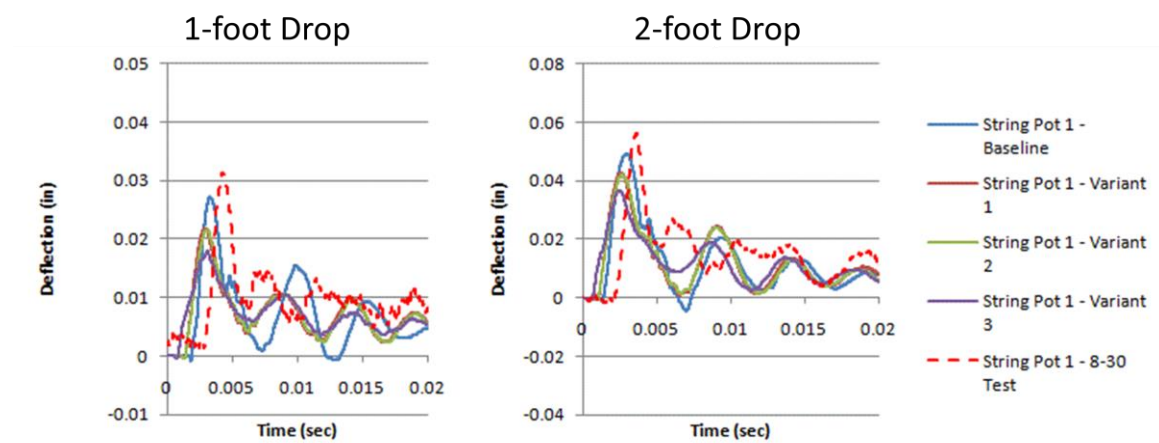
Figure 45. String Pot 1 Deflection Histories for Water Model Variants

The histories of the von Mises stresses at Strain Gage 2 are illustrated in Figure 46. The baseline water model again produced the highest initial peak, and best matched the test data.
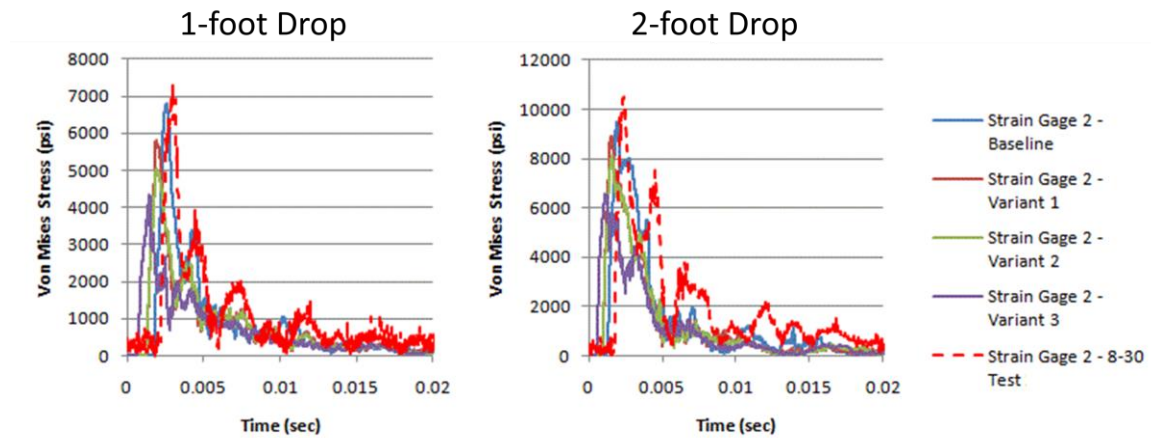
Figure 46. Strain Gage 2 Von Mises Stress Histories for Water Model Variants

The simulations for the 1-foot drops predicted no plastic strain. The simulation of the 2-foot drop with the baseline water model predicted a small region of plastic strain at the outer surface of the tank head at the apex. The other water model variants did not predict a significant region of plastic strain. Contours of the plastic strain at the conclusions of the simulations for the water model variants are shown in Figure 47.
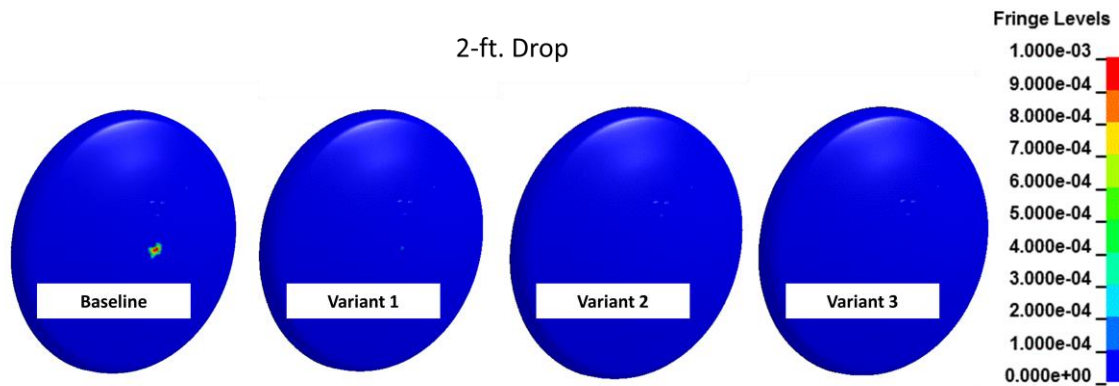
Figure 47. Plastic Strain Contours for Water Model Variants for 2-foot Drops

Figure 48 shows the penetration of the fluid through the coupling interface at 0.003 seconds after impact. The baseline water model shows a nearly continuous zone of penetration across the contact patch. The other variants show at most a ring of penetration at the perimeter of the contact patch.

35

1-ft. Drop

2-ft. Drop
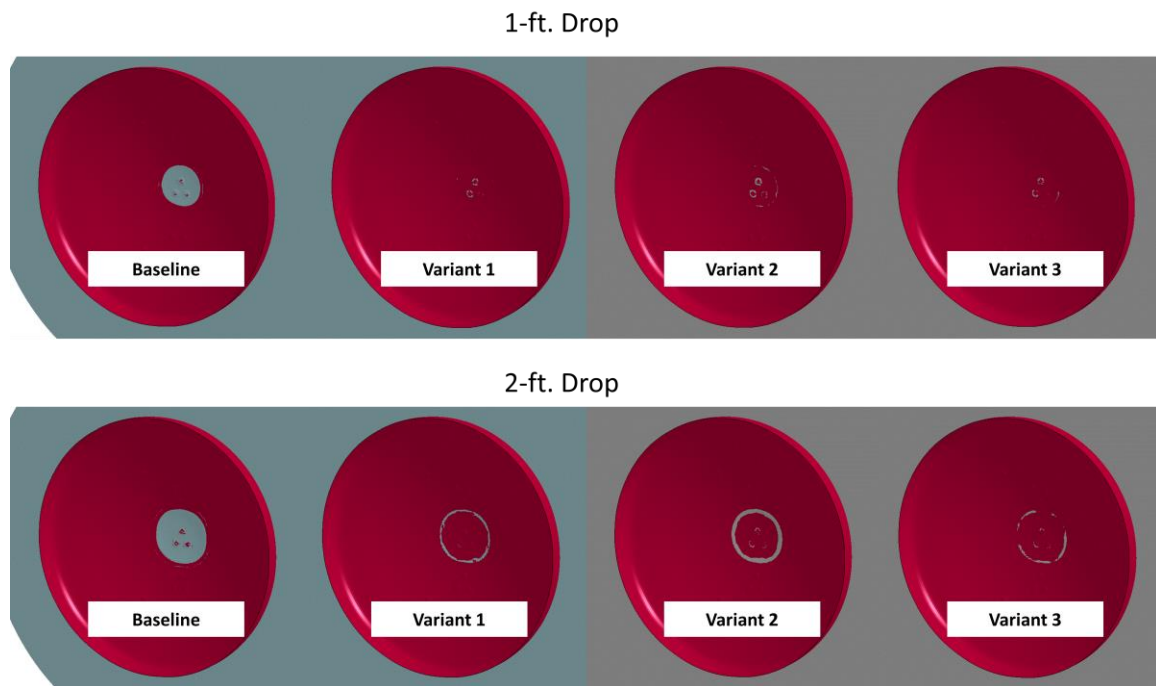
Figure 48. Fluid Penetration through Coupling Interface 0.003 seconds after Impact for Water Model Variants

The baseline water model produced acceleration, deflection, and stress results that are in better agreement with test data than the variants. As a consequence, this was the water model chosen for further comparisons with test data.

6.5 Sensitivity to Structural and Water Mesh Density

The baseline simulation model was used for comparison against data from two tests each at drop heights of 1 foot and 2 feet. The baseline model featured an element size of 0.2" for both the structure and the water mesh in the region of the initial impact. Variants were created with element sizes of 0.1", 0.4" and 0.8". All the models used the Curve 11 x 1 coupling stiffness and 50% coupling surface damping. The 0.1" and 0.2" water meshes featured biased meshes with element sizes that increased both toward the outer perimeter and toward the bottom of the water block. The 0.4" and 0.8" water meshes featured a fairly uniform element size with an irregular element pattern across the surface. The model variants are illustrated in Figure 49.
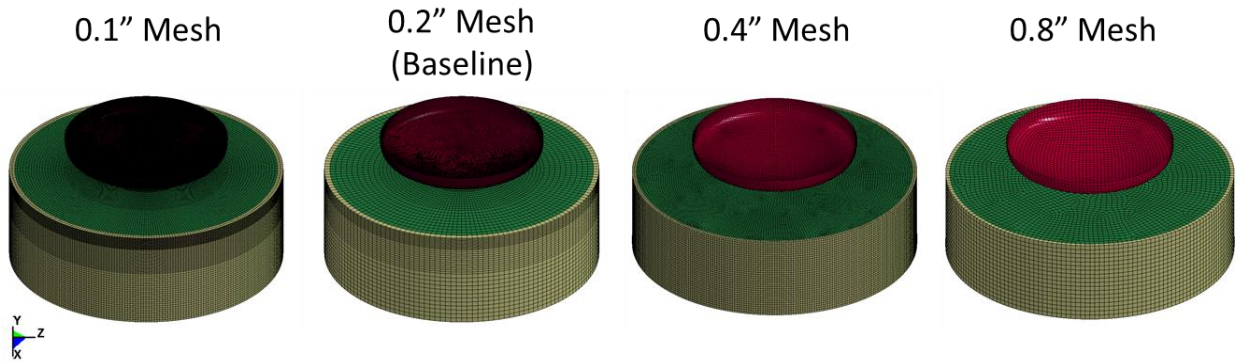
Figure 49. Mesh Density Model Variants

Von Mises stress contours at the inner surface at 0.003 seconds are illustrated in Figure 50. The 0.1" and 0.2" mesh variants show nearly identical responses, which suggests that any mesh refinement beyond 0.2" is unnecessary. For an engineering evaluation of the adequacy of the structure, the results from the 0.8" mesh would probably be adequate.
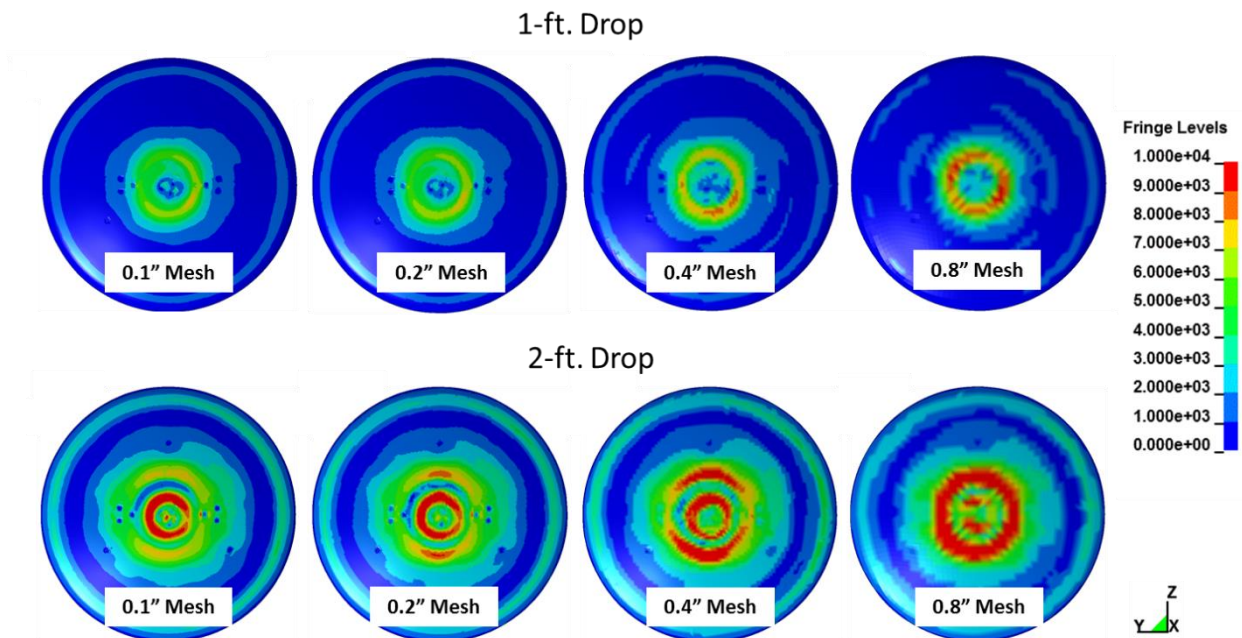
Figure 50. Von Mises Stress at the Inner Surface 0.003 seconds After Impact for Mesh Density Variants

Contours of the plastic strain predicted from the 2-foot drops are illustrated in Figure 51. The plastic strain distributions for the 0.1" and 0.2" meshes are nearly identical, and the distribution for the 0.4" mesh is similar though the peak magnitude is lower. The plastic strain distribution for the 0.8" clearly differs from the others.

37
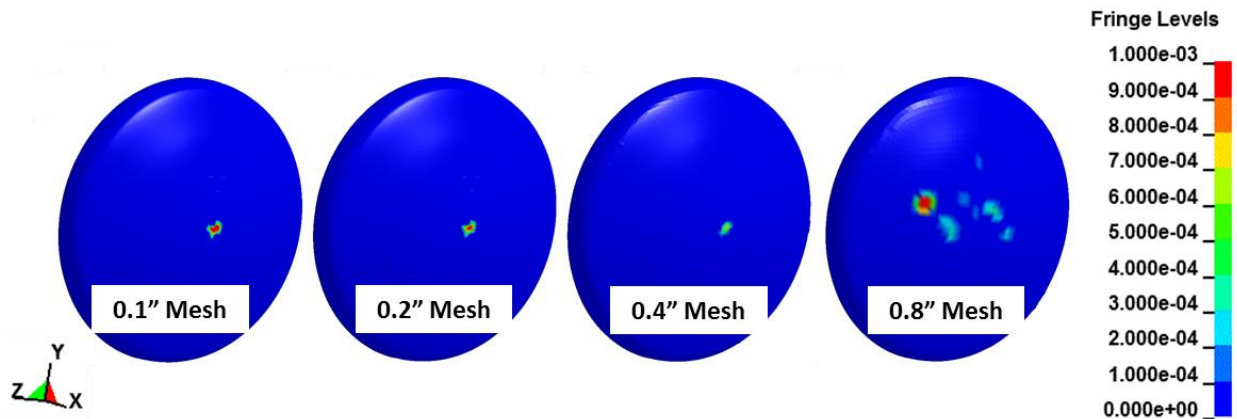
Figure 51. Plastic Strain for Mesh Density Variants for 2-foot Drops

Contours of the pressure acting on the outer surface of the tank head are illustrated in Figure 52. Again, the response for the 0.2" mesh is very similar to the 0.1" mesh, which suggests that no additional mesh refinement is necessary. Even the 0.8" mesh shows a strong coliseum effect. It is anticipated that the fluid-structure coupling stiffness should increase as the element size decreases. These results suggest that the sensitivity of the response to the coupling stiffness is not so strong as to be a concern for the range of element sizes utilized in this study.
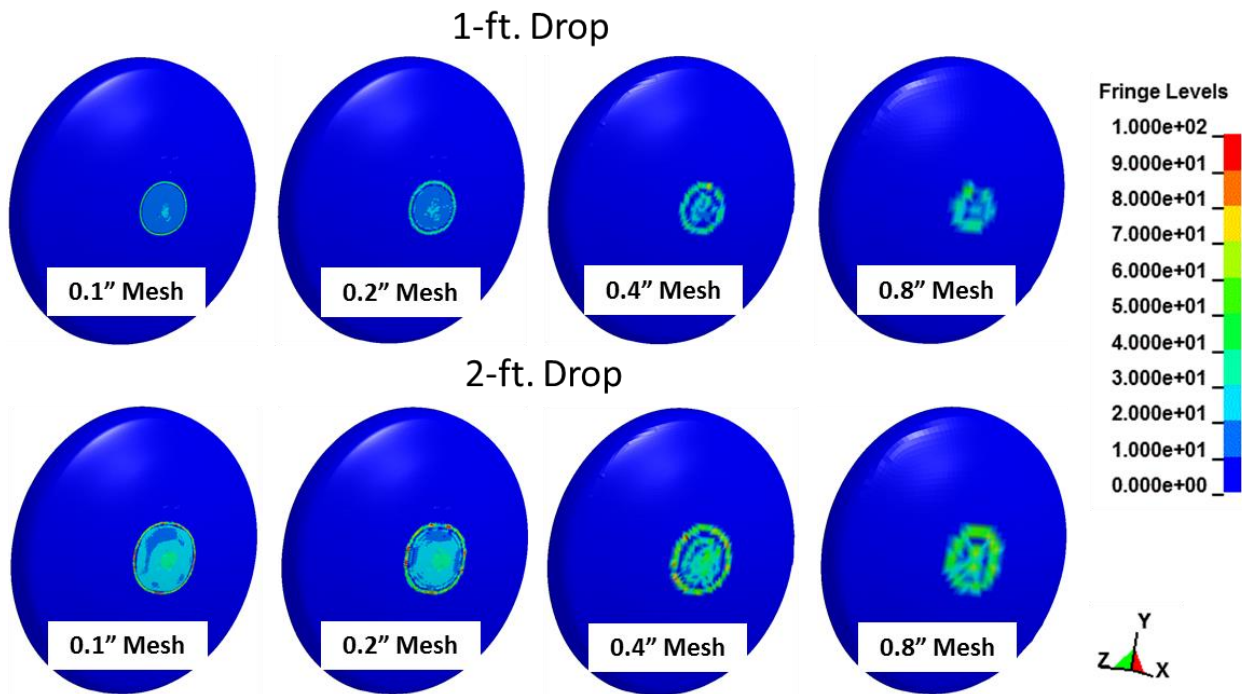
Figure 52. Interface Pressure 0.003 seconds After Impact for Mesh Density Variants

38

Figures 53 show comparisons of acceleration histories for each of the variants along with data from the 8/30 Test 1 (1-foot drop) and 8/30 Test 2 (2-foot drop). The time histories show that all the variants closely track the first peak of the acceleration history. The 0.8" mesh is first to diverge from the test data, but still gives results that are acceptable for engineering evaluation of the adequacy of the structure.
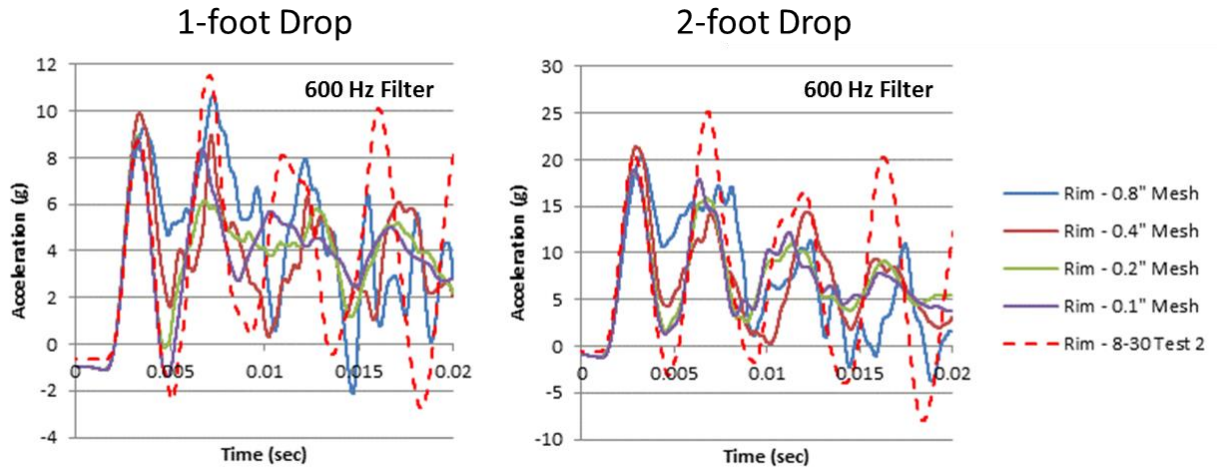
Figure 53. Acceleration Histories for Mesh Density Variants

Figure 54 illustrates pressure histories at Gage 7. The 0.1" and 0.2" mesh pressure histories follow the general character of the test measurement in having a sharp spike followed by a broad hump, but the magnitudes do not match. The area for the pressure measurement in the simulations is the size of one structural element, which for the 0.1" mesh is similar to the size of the one-eighth inch diameter head of the pressure transducers, so the difference in area over which the pressure is measured does not explain the difference between the test measurement and simulation prediction. Part of the explanation for the discrepancy is that the fluid-structure modeling algorithm in the LS-DYNA is an approximate method that does not model the full physics of the fluid flow problem.
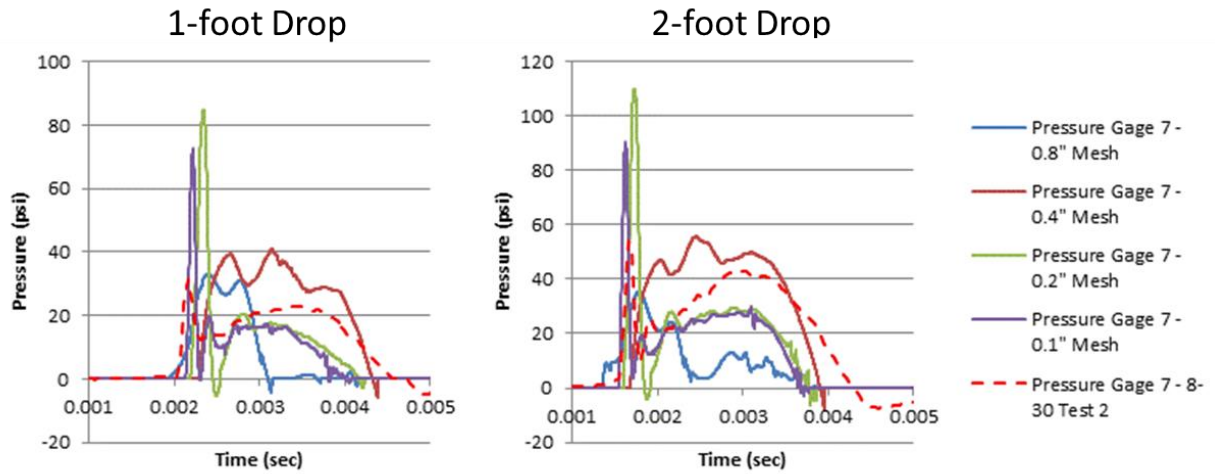
Figure 54. Gage 7 Pressure Histories for Mesh Density Variants

Figure 55 illustrates deflection histories for String Pot 1. All the mesh variants track reasonably well with the test response through the first peak. The 0.8" mesh actually provided the closest prediction for the peak response.
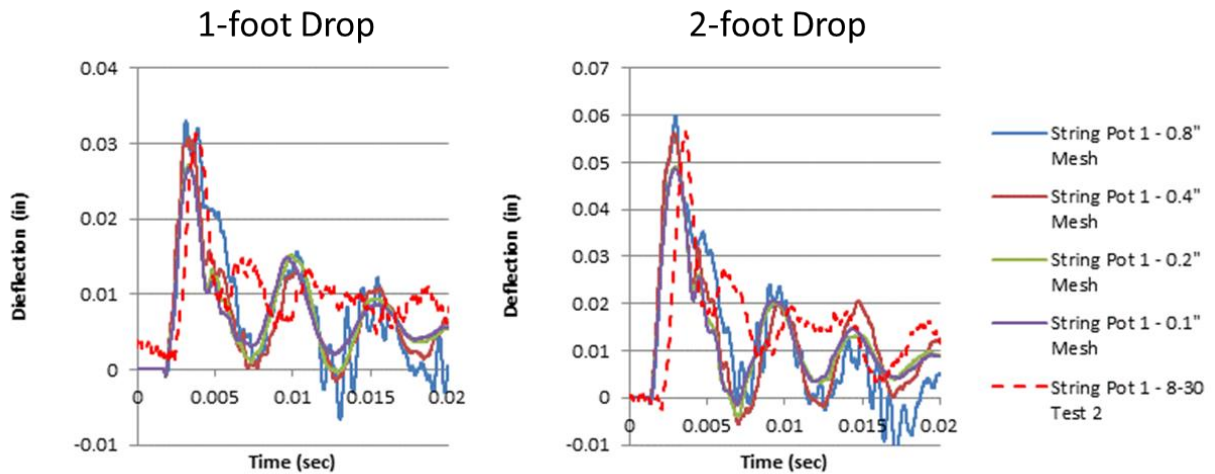
Figure 55. String Pot 1 Deflection Histories for Mesh Density Variants

Stresses for the mesh variants are shown in Figure 56. Again, all the mesh variants closely track the test response through the first peak. Even the 0.8" mesh would be adequate for engineering evaluation of the adequacy of the structure. The mesh density of the 0.2" baseline mesh was not a limiting factor in the correlation with test data. The 0.1" mesh did not provide any significant benefit to justify the increase in disk space and solution time.

40
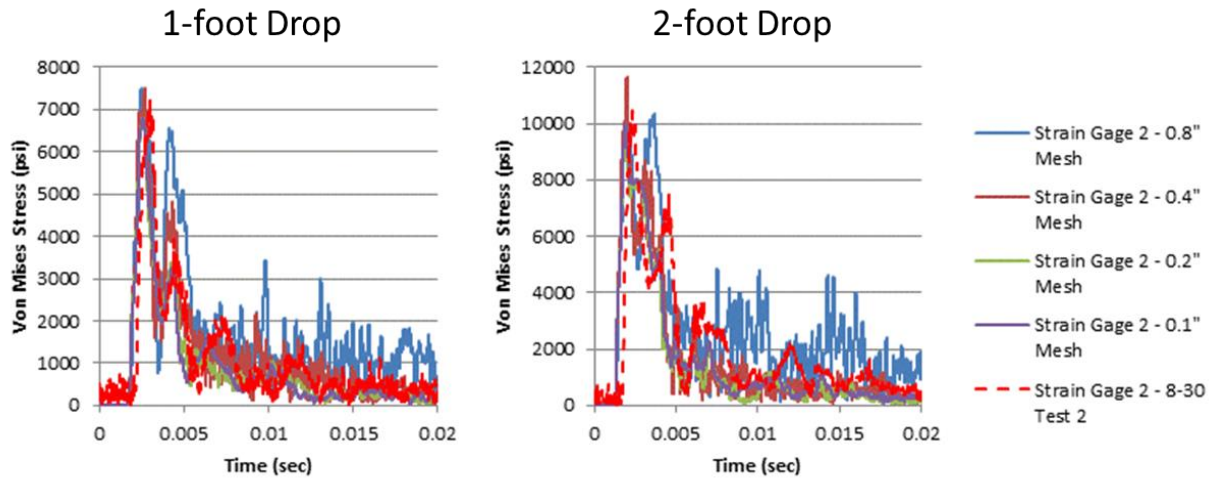
Figure 56. Strain Gage 2 Von Mises Stress Histories for Mesh Density Variants

7. Test versus Simulation Comparisons

7.1. Simulation Model and Test Data for Comparisons

The baseline simulation model was used for comparison against data from two tests each at drop heights of 1 foot and 2 feet. The baseline model featured Curve 11 x 1 coupling stiffness, 50% coupling surface damping, and a fluid element size of approximately 0.2 inches in way of the initial impact.

For 1-foot drops, 8-27 Test 1 and 8-30 Test 1 were used for acceleration comparisons, and 8-30 Test 1 and 9-10 Test 1 were used for pressure, deflection, and stress comparisons. For 2-foot drops, all comparisons were made using data from 8-30 Test 2 and 8-30 Test 3.

7.2. Acceleration

Acceleration histories are illustrated in Figures 57 and 58 for 1-foot and 2-foot drops. The acceleration histories were shifted so that the initial peaks approximately align. The results show that the initial peaks were well predicted by the simulations; however, later peaks were generally under-predicted. The results also show that the tests were very repeatable.
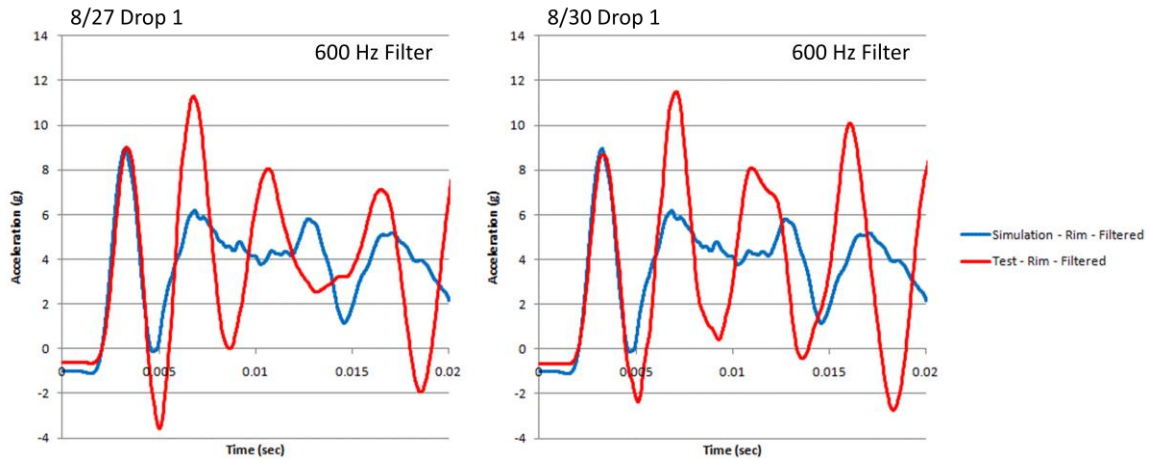
Figure 57. Acceleration Histories for 1-foot Drops
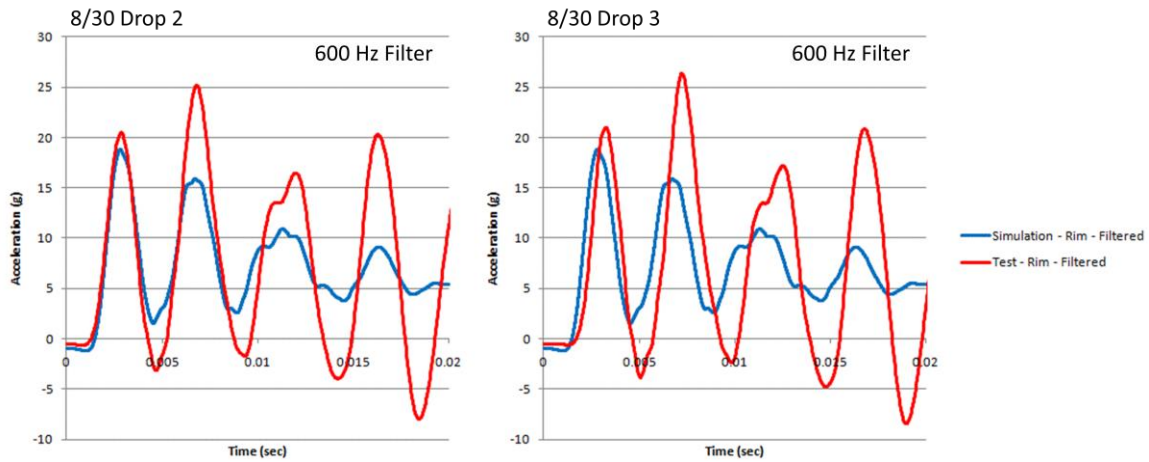
Figure 58. Acceleration Histories for 2-foot Drops

7.3. Pressure

Figures 59 through 62 illustrate the pressure histories for 1-foot drops. Figures 63 through 66 illustrate the pressure histories for 2-foot drops. The pressure histories are grouped based on the distance the gages are from the apex. Gages 7 through 8 are closest to the apex, followed by 6 and 12, then 4, 5, 10 and 11, and finally 1 through 3. Several observations can be made regarding the pressure histories.

- The pressure histories from the tests are highly repeatable.
- The tank head impacts with negligible pitch angle as evidenced by the near simultaneous arrival of the pressure pulse at Gages 7 through 9.
- The pressure histories from the tests are characterized by a sharp peak preceded and/or followed by a lower frequency pressure oscillation. The lower frequency

42

oscillations show a half-sine wave duration of 0.002 seconds, which corresponds to 250 Hz, which corresponds to the first flexural mode of the tank head.

- The LS-DYNA simulations are characterized by sharp initial pressure peaks. The peaks are sometimes trailed by low frequency oscillations, but are never preceded by low frequency oscillations.
- The LS-DYNA simulation consistently over-predicted the magnitudes of the pressure peaks.
- The initial peaks of the LS-DYNA simulations show the same timing as the sharp peaks of the tests. For instance, the tests show the sharp peak in the pressure occurring at Gage 12 before Gage 6 even though they are at the same distance from the apex. The LS-DYNA simulation shows the same timing. Similar differences in the sharp peak of the pressure pulse are seen between the right side Gages 10 and 11 and the left side Gages 4 and 5. The difference in timing between the right and left sides of the model is probably due to flexure. The LS-DYNA simulations show negligible pitching of the tank head.
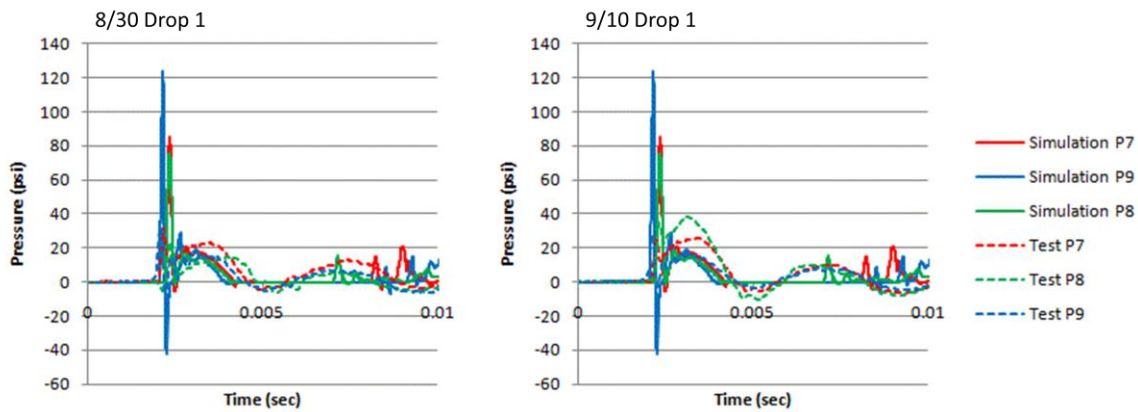
Figure 59. Pressure Histories at Gages 7 through 9 for 1-foot Drops
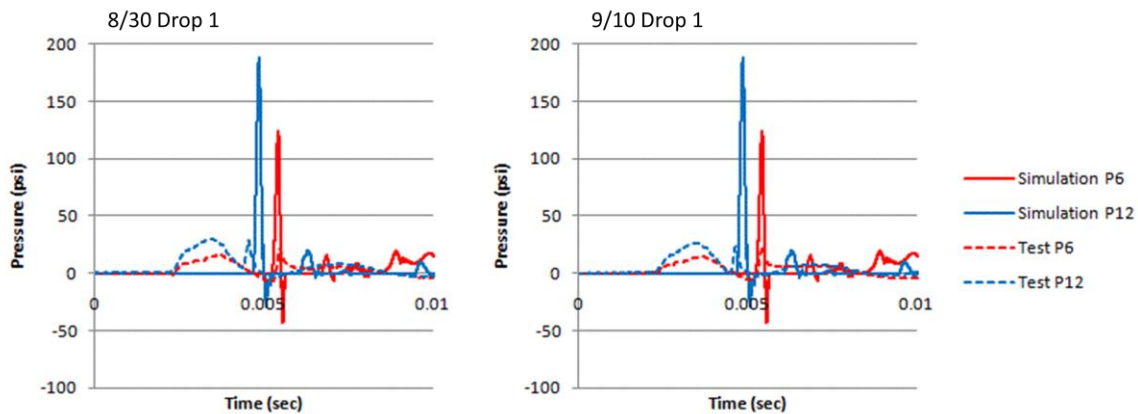
Figure 60. Pressure Histories at Gages 6 and 12 for 1-foot Drops
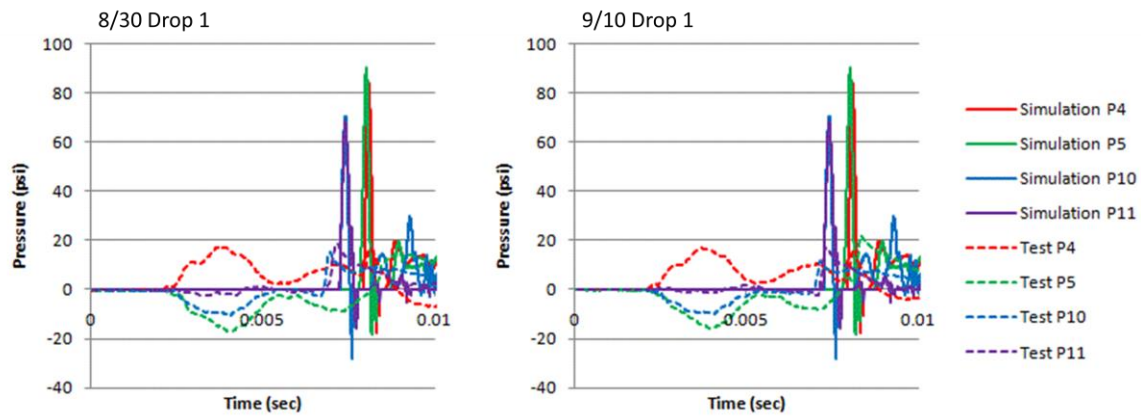
Figure 61. Pressure Histories at Gages 4, 5, 10, and 11 for 1-foot Drops
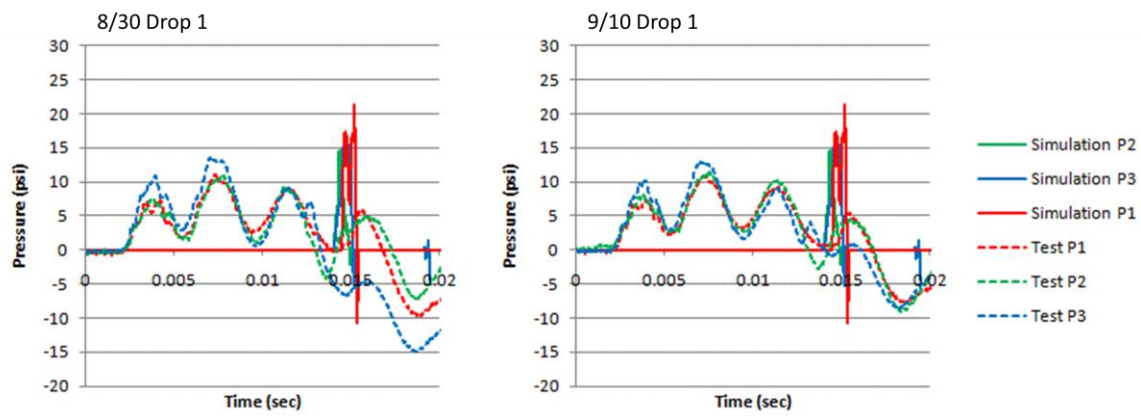
Figure 62. Pressure Histories at Gages 1 through 3 for 1-foot Drops
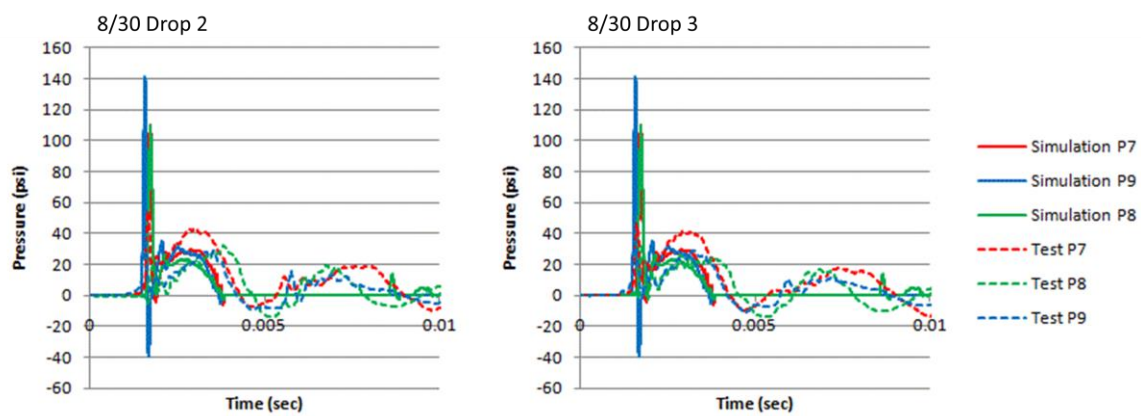
Figure 63. Pressure Histories at Gages 7 through 9 for 2-foot Drops

44
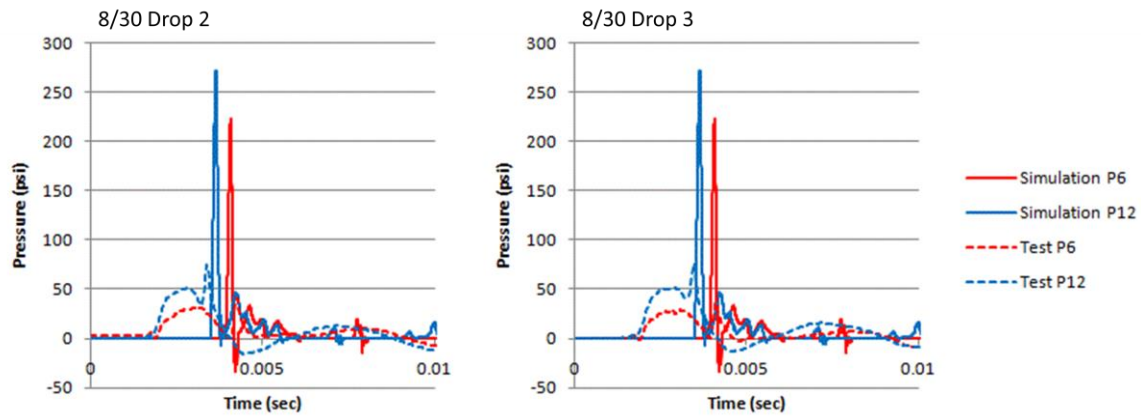
Figure 64. Pressure Histories at Gages 6 and 12 for 2-foot Drops
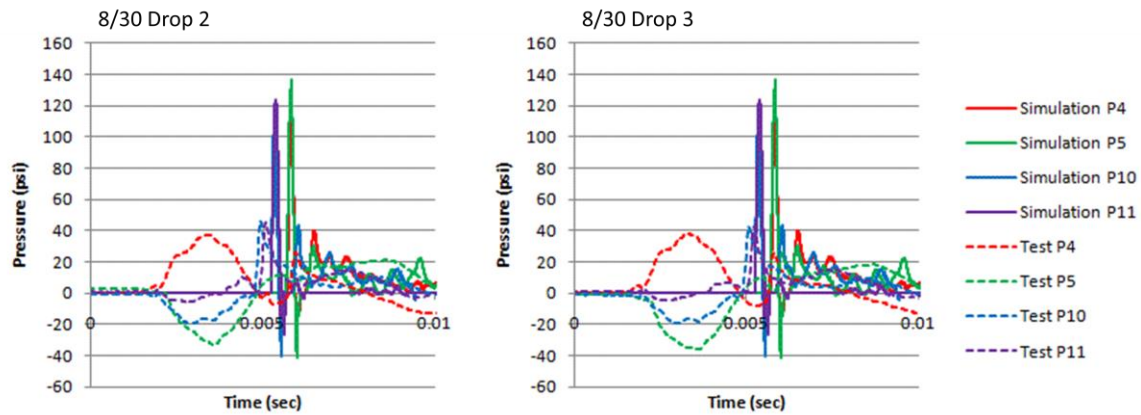
Figure 65. Pressure Histories at Gages 4, 5, 10, and 11 for 2-foot Drops
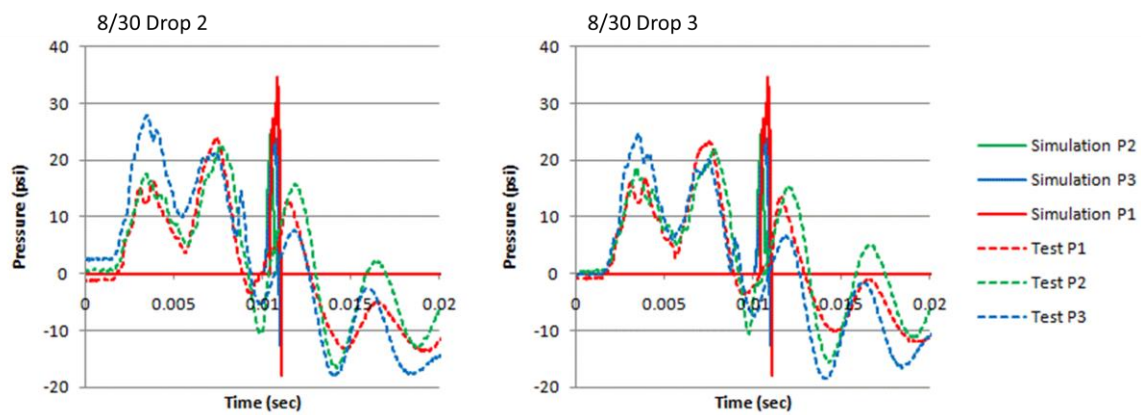
Figure 66. Pressure Histories at Gages 1 through 3 for 2-foot Drops

7.4. Deflection

Deflection time histories for 1-foot drops are shown in Figure 67, and 2-foot drops in Figure 68. The time histories for the test data were filtered by computing a 0.25 millisecond running average, which filtered out the high frequency noise. This filtering was not absolutely necessary as the amplitude of the noise is low and does not obscure the shape of the time histories. The filtering was done only to make it easier to distinguish the individual curves. The time histories show that the tests are very repeatable. String Pot 2 consistently shows a much higher deflection amplitude than String Pots 1 and 3. The peak deflection magnitudes from String Pots 1 and 3 are similar to the simulations; however, the time histories are significantly different. The string pot histories initially lag the simulation histories and reach higher peaks. String Pot 2 reaches the highest peak and rebounds past zero. This may be due to the dynamics of the string pots. The string pots features a spring-loaded reel that is mounted to the cover plate. A string extends from the reel to a hook on mounted on the tank head. The spring stiffness together with the rotary inertia of the reel forms an oscillatory system. For deflections that occur in the time frame of the impact tests, the string pot dynamics may have an effect on the deflection readings.
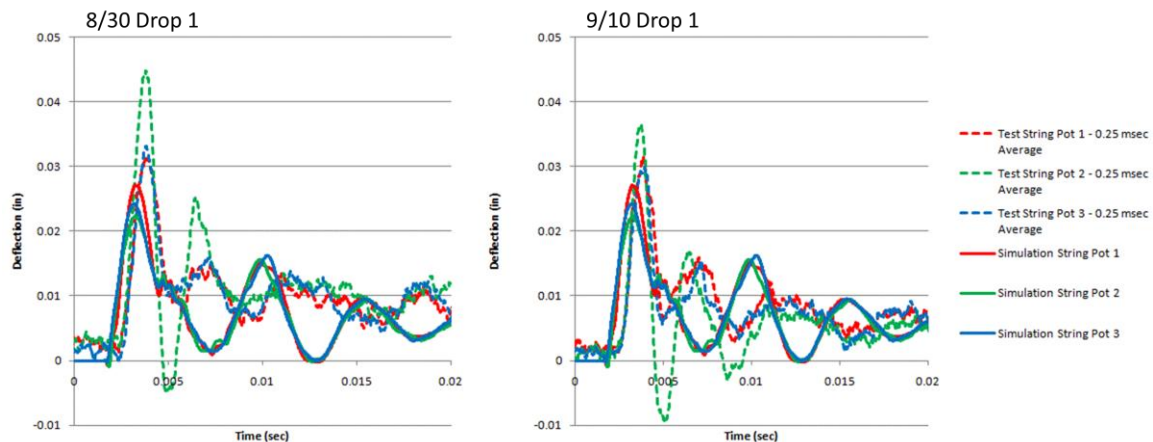
Figure 67. Deflection Histories for 1-foot Drops
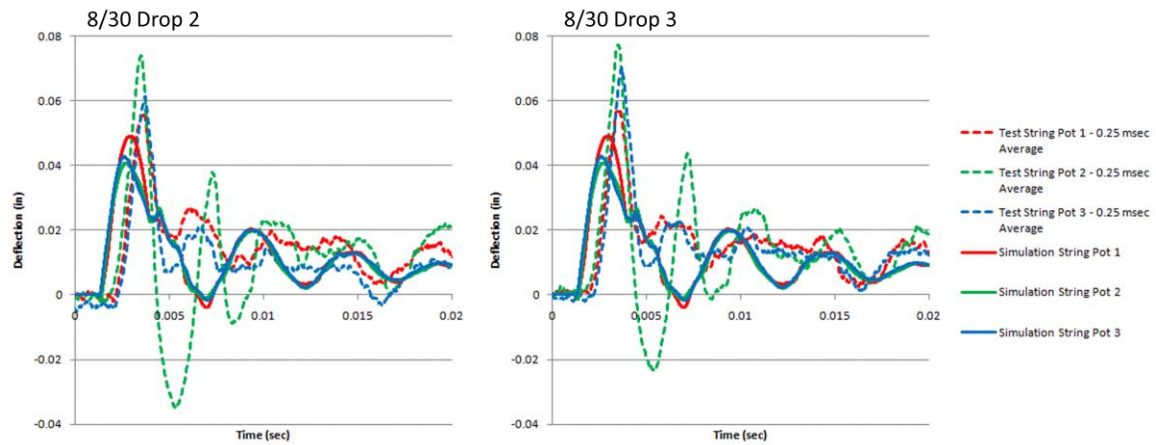
Figure 68. Deflection Histories for 2-foot Drops

7.5. Stress

Test and simulation stress histories are compared for 1-foot drops in Figures 69 and 70. Stress histories are compared for 2-foot drops in Figures 71 and 72. Despite being located symmetrically opposite each other, Strain Gage 2 consistently reads higher than Strain Gage 3. Similarly, Strain Gage 4 consistently reads higher than Strain Gage 1. Strain Gages 2 and 4 are on opposite sides of the tank head, so this could not be explained by pitching of the tank head to one side. The peak magnitudes and time durations for Strain Gages 1 and 2 are very similar to the simulations; however, the timing of the stress peaks in the tests lags the simulations.
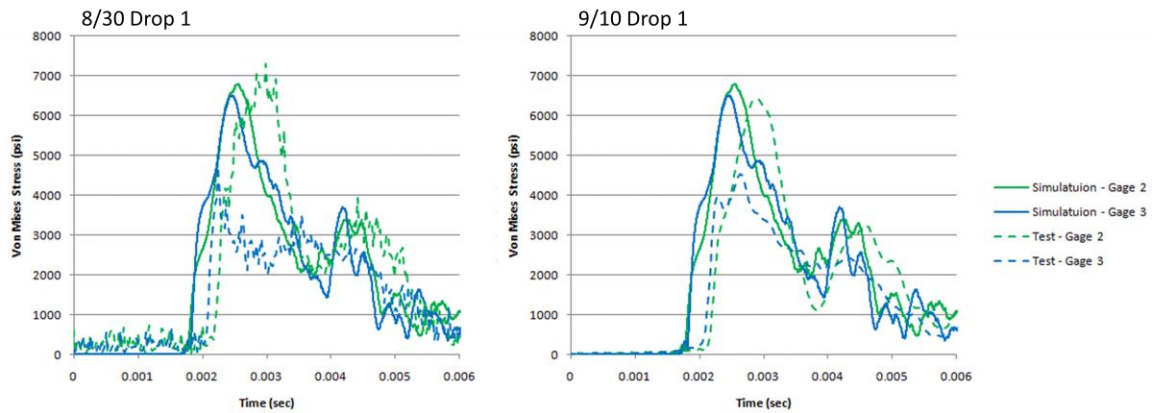
Figure 69. Stress Histories for Strain Gages 2 and 3 for 1-foot Drops

47
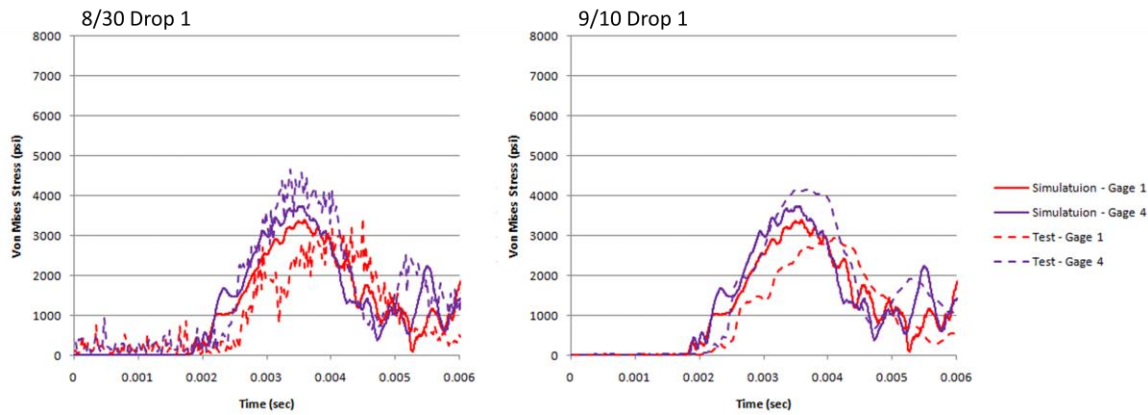
Figure 70. Stress Histories for Strain Gages 1 and 4 for 1-foot Drops
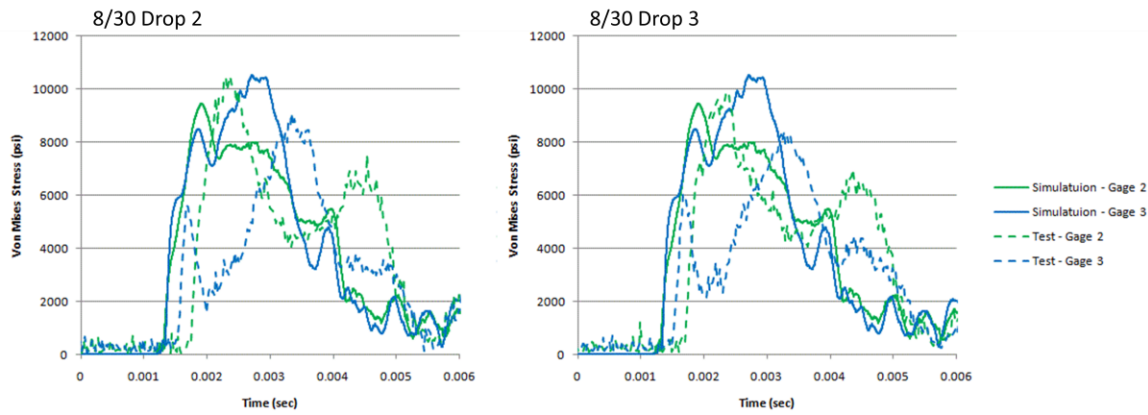
Figure 71. Stress Histories for Strain Gages 2 and 3 for 2-foot Drops
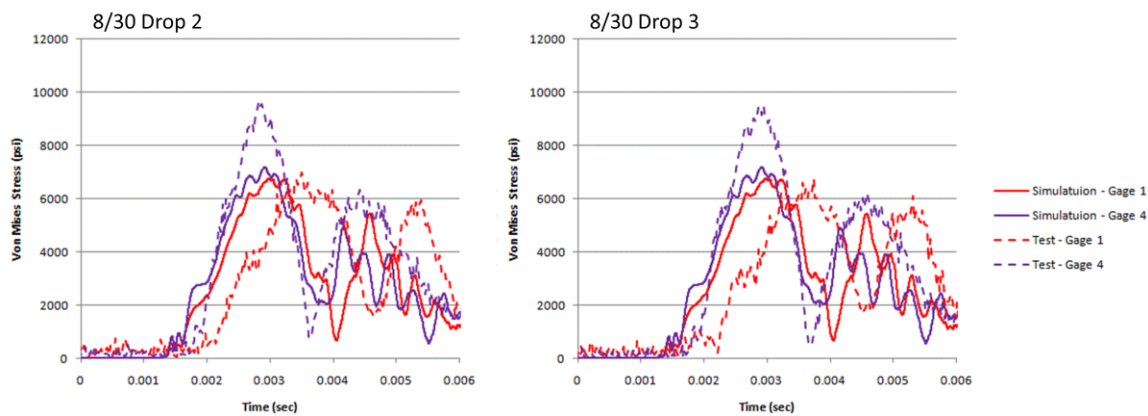
Figure 72. Stress Histories for Strain Gages 1 and 4 for 2-foot Drops

48

7.6. Plastic Strain

The simulation for the 1-foot drop predicted no plastic strain. The simulation for the 2-foot drop predicted a small region of plastic strain at the outer surface of the tank head at the apex. Contours of the plastic strain at the conclusion of the simulation are shown in Figure 73. The peak plastic strain is 0.001148 in/in.
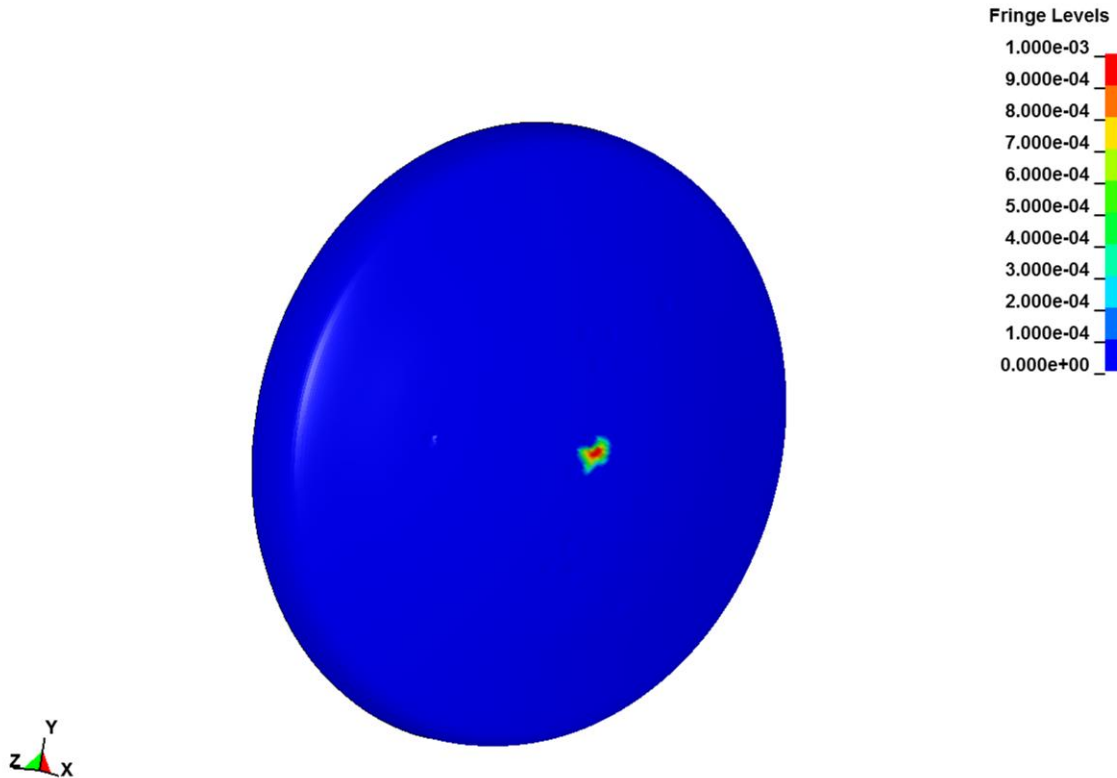
Figure 73. Plastic Strain Contours for Simulation of 2-foot Drop

There is no direct measurement available of plastic strain from the tests; however, there is evidence of some permanent deformation based on scans of the surface that were made before and after the test series. The relative difference of the surface measurements are shown in Figure 74. This is the deformation accumulated over the entire test series. The surface scans show that the deformation is 0.006 inches at the apex. The peak negative deformation is -0.004 inches at three O'clock. The peak positive deformation is 0.008 inches at seven O'clock.
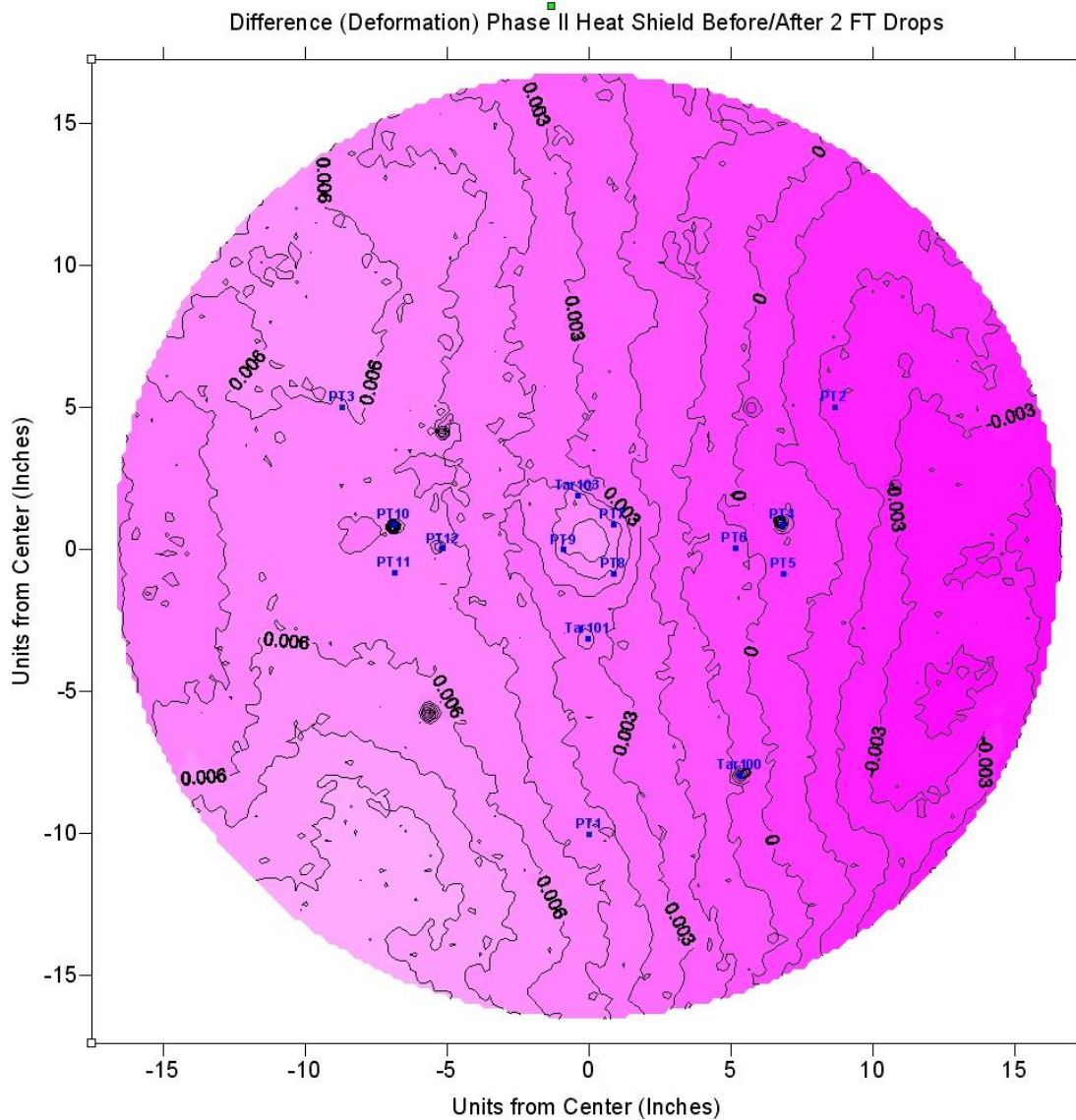
Figure 74. Deformation Contours as Determined form Pre-Test and Post-Test Surface Scans

8. Simulation Prediction Accuracy

As a measure of the simulation accuracy, the peak simulation responses were compared to the peak test responses. The absolute values of the peaks were used for the comparison irrespective of the timing and sign (positive or negative). The rationale for this approach is that structural design development is generally based on peak responses. The correlation was based on the baseline model with 0.2" mesh, Curve 11 coupling stiffness, and 50% critical damping for the fluid-structure coupling. Figures 75 through 78 illustrate the test peak versus simulation peak comparisons for acceleration, pressure, deflection, and von Mises stress. It is immediately apparent from the plots that the

50

acceleration and deflection predictions are biased low, the pressure predictions are biased high, and the stress predictions show no significant bias. The pressure predictions with the lowest values show no bias. These are at the pressure gages farthest from the apex. Simulation versus test correlation is poorest for the highest pressures near the apex.
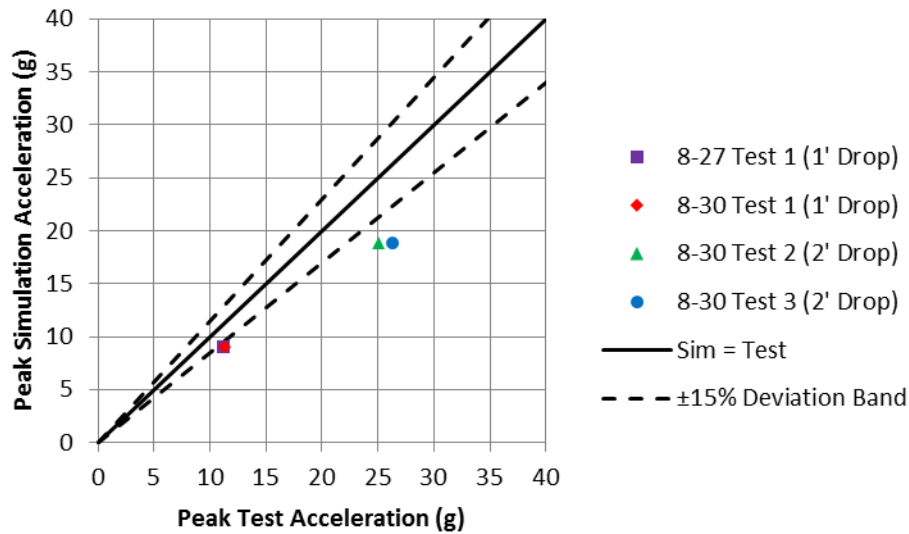
Figure 75. Peak Test Acceleration vs. Peak Simulation Acceleration
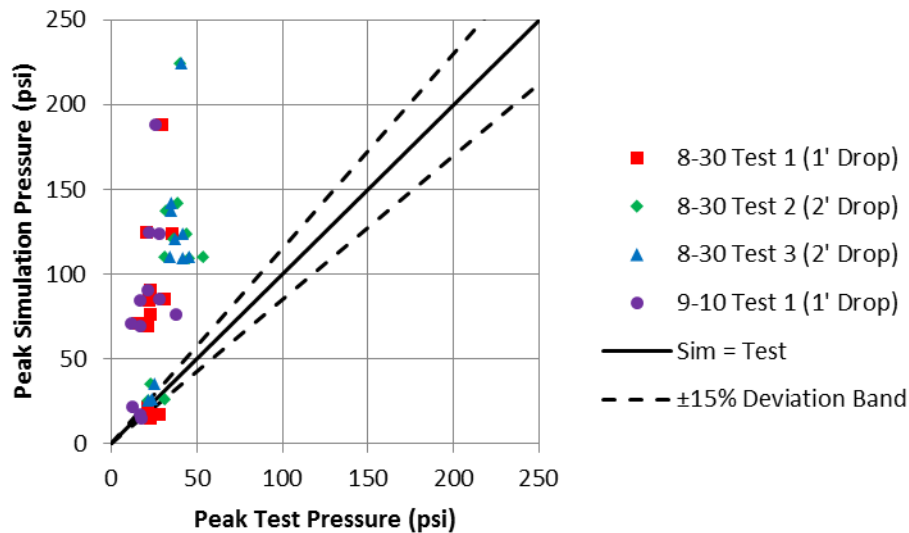
Figure 76. Peak Test Pressure vs. Peak Simulation Pressure

51
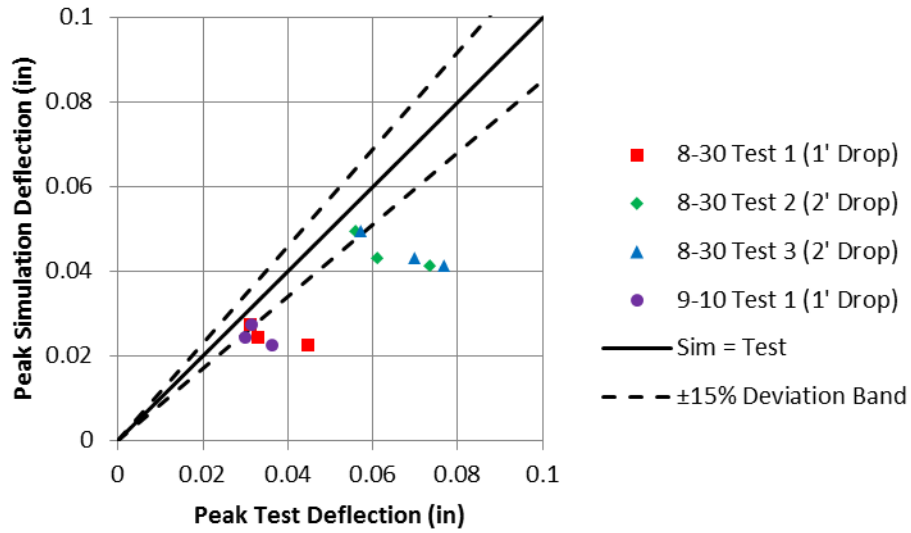
Figure 77. Peak Test Deflection vs. Peak Simulation Deflection
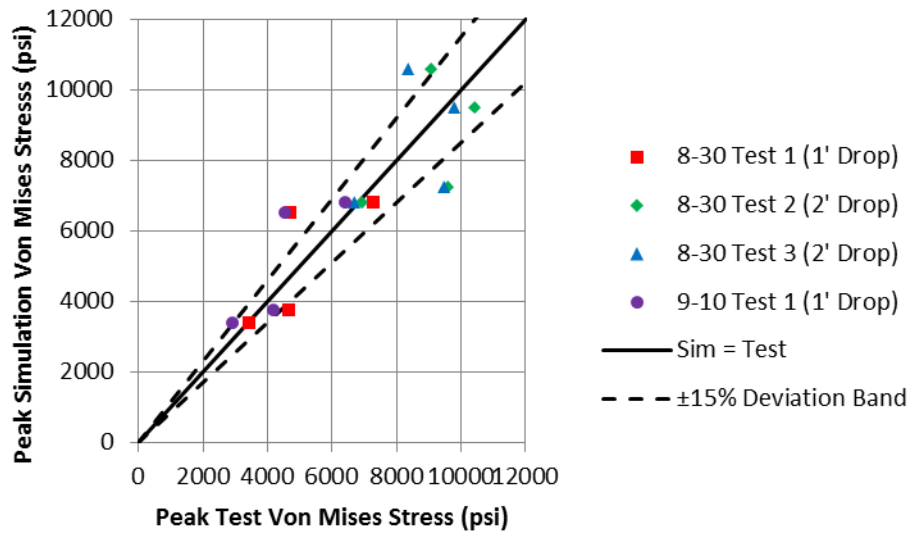
Figure 78. Peak Test Von Mises Stress vs. Peak Simulation Von Mises Stress

In order to quantify the correlation, the averages of the absolute values of the percentage deviations were computed. These are summarized in Table 5.

Table 5. Average Absolute Percentage Deviations

Parameter	Average Absolute Percentage Deviation
Acceleration	24.2
Pressure	222.2
Deflection	29.2
Stress	15.5

9. Conclusions and Recommendations

The results for the tank head model demonstrated the following.

1. LS-DYNA can provide reasonable predictions for acceleration, deflection, and stress time histories for a broad range of fluid-structure coupling parameters.
2. LS-DYNA acceleration, deflection, and stress time histories converge as mesh density increases.
3. LS-DYNA coupling pressure time histories are highly dependent on fluid-structure coupling parameters.
4. LS-DYNA coupling pressure time histories do not necessarily converge as mesh density increases.

The results from the correlation of test and simulation data show that the principal objectives of the tests were met. The test data for accelerations, stresses, displacements, and pressure was usable for the correlation effort. The test article did feature enough flexure to produce meaningful strains and affect the pressure time histories.

References

[1]   Hallquist, J.O., "LS-DYNA Theoretical Manual", LSTC Livermore, 1998.
[2]   Vassilakos, Gregory J., "Simulation of Elemental Water Impact Tests of a 20-inch Penetrometer," LRC-SPL-PL-068, November 10, 2010.
[3]   Stegall, David E., LRC-SPL-PL-000, "Elemental Water Impact Test, Phase 2A Test Report, Two Foot Drop Set", Date TBD.
[4]   Templeton, Justin D. and Rice, Chad E., "Elemental Water Impact Testing (EWIT) Modal Test Report," September 28, 2010.
[5]   "LS-DYNA Keyword User's Manual, Version 971," Livermore Software Technology Corporation, May 2007.
[6]   Wilkinson, J.P.D., "Study of Apollo Water Impact, Final Report, Volume 4, Comparison with Experiments," SID 67-498, North American Aviation, Inc., May 1967.

Appendix A. LS-DYNA Model

The following are the LS-DYNA cards that control the material properties, contact, and initial conditions for the axisymmetric model. These particular cards are for a 1-foot drop with the Curve 11 coupling stiffness and 50% critical damping.

```
*KEYWORD 800000000
$  Lobatto integration with 10 points through thickness
$  50% coupling damping
*TITLE
3D AS-BUILT MODEL OF 36-INCH TANK HEAD
*CONTROL_TERMINATION
$    ENDTIM     ENDCYC      DTMIN     ENDENG     ENDMAS
    0.02000                   0.0        0.0        0.0
$*CONTROL_PARALLEL
$4
*CONTROL_HOURGLASS
         1        0.1
*CONTROL_ENERGY
$#     HGEN       RWEN     SLNTEN      RYLEN
         2          2
*CONTROL_OUTPUT
$#    NPOPT     NEECHO     NREFUP     IACCOP      OPIFS     IPNINT     IKEDIT     IFLUSH
         1          3
$#    IPRTF
         0
$
*DATABASE_GLSTAT
 0.0000020
*DATABASE_MATSUM
 0.0000020
*DATABASE_NODOUT
 0.0000020
*DATABASE_ELOUT
 0.0000020
*DATABASE_HISTORY_NODE
$      id1        id2        id3        id4        id5        id6        id7        id8
$     apex   cover cl  cover -y  cover sp1 cover sp2 cover sp3  head sp1  head sp2
   4419374    4477728    4478729    4478897    4478228    4477731    4419312    4432185
$ head sp3   ring -y    ring +y    ring -z    ring +z
   4418835    4477172    4477451    4477434    4477297
*DATABASE_HISTORY_SHELL
$      id1        id2        id3        id4        id5        id6        id7        id8
$      sg1        sg2        sg3        sg4
   4056184    4052352    4054022    4000706
*DATABASE_BINARY_D3PLOT
$#       dt       lcdt       beam      npltc
$ 0.0000200       7778
     0.0002
*DATABASE_BINARY_FSIFOR
$        dt
$ 0.0000200       7778
     0.0002
*DATABASE_FSI
$        dt
 0.000002
$ dbfsi_id        sid    sidtype       swid      convid
$        10         10          2
         11         11          2
         12         12          2
         13         13          2
         21         21          2
         22         22          2
         23         23          2
         31         31          2
         32         32          2
         33         33          2
         41         41          2
         42         42          2
         43         43          2
*DATABASE_BINARY_D3THDT
   999.999
$
```

```
*CONTACT_AUTOMATIC_SURFACE_TO_SURFACE
$     ssid      msid     sstyp     mstyp    sboxid    mboxid       spr       mpr
        10        11         3         3
$       fs        fd        dc        vc       vdc    penchk        bt        dt

$      sfs       sfm       sst       mst      sfst      sfmt       fsf       vsf

$     soft     sofscl    lcidab    maxpar     sbopt     depth     bsort    frcfrq

$   penmax     thkopt    shlthk     snlog      isym     i2d3d    sldthk    sldstf

$     igap     ignore    dprfac    dtstif                                 flangl
                    1
*CONTACT_AUTOMATIC_SURFACE_TO_SURFACE
$     ssid      msid     sstyp     mstyp    sboxid    mboxid       spr       mpr
         6        11         3         3
$       fs        fd        dc        vc       vdc    penchk        bt        dt

$      sfs       sfm       sst       mst      sfst      sfmt       fsf       vsf

$     soft     sofscl    lcidab    maxpar     sbopt     depth     bsort    frcfrq

$   penmax     thkopt    shlthk     snlog      isym     i2d3d    sldthk    sldstf

$     igap     ignore    dprfac    dtstif                                 flangl
                    1
*SET_PART_LIST
         1
         2         3        22        23
*SET_PART_LIST
       222
         2        22
*SET_PART_LIST
       323
         3        23
*ALE_MULTI-MATERIAL_GROUP
$      sid    idtype
       222         0
       323         0
*SET_MULTI-MATERAIL_GROUP_LIST
       123
         2
*CONTROL_ALE
$#     dct      nadv      meth      afac      bfac      cfac      dfac      efac
         2         1         2      -1.0
$#   start       end     aafac     vfact      prit       ebc      pref    nsidebc
                                                                  14.7
$
*CONSTRAINED_LAGRANGE_IN_SOLID
$#   slave    master     sstyp     mstyp     nquad     ctype     direc     mcoup
         6         1         1         0         2         4         2      -123
$#   start       end      pfac      fric    frcmin      norm   normtyp      damp
         0         0       -11         0         0         0         0      0.50
$#      cq      hmin      hmax     ileak     pleak   lcidpor     nvent    iblock
         0         0         0         0       0.1
$#  iboxid    ipenchk   intforc    ialesof    lagmul    pfacmm      thkf
         0         0         1         0         0
$
*DEFINE_CURVE
$     lcid      sidr       sfa       sfo
        11                 1.0      1.00
               0.000                 0.0
               0.020               200.0
$
*CONTROL_SHELL
$   wrpang     esort     irnxx     istupd    theory       bwc     miter      proj

$  rotascl    intgrd    lamsht    cstyp6    tshell    nfail1    nfail4   psnfail
                    1
*SECTION_SHELL
$      SID    ELFORM      SHRF       NIP     PROPT        QR     ICOMP
         6        16   0.83333        10       1.0       0.0
$       T1        T2        T3        T4      NLOC     MAREA
    0.0001    0.0001    0.0001    0.0001       0.0       0.0
*SECTION_SHELL
$      SID    ELFORM      SHRF       NIP     PROPT        QR     ICOMP
         9        16   0.83333         2       1.0       0.0
```

55

```
$        T1          T2          T3          T4        NLOC       MAREA
        0.50        0.50        0.50        0.50         0.0         0.0
*SECTION_SHELL
$       SID      ELFORM        SHRF         NIP       PROPT          QR       ICOMP
         10          16     0.83333           2         1.0         0.0
$        T1          T2          T3          T4        NLOC       MAREA
        0.50        0.50        0.50        0.50         0.0         0.0
*SECTION_SOLID
$       SID      ELFORM
         11           1
*SECTION_BEAM
$     secid      elform        shrf          qr         cst       scoor         nsm
         12           1     0.83333           2           1           0          0.
$       ts1         ts2         tt1         tt2       nsloc       ntloc
       0.250       0.250          0.          0.           0           0
*SECTION_BEAM
$     secid      elform        shrf          qr         cst       scoor         nsm
         14           1     0.83333           2           1           0          0.
$       ts1         ts2         tt1         tt2       nsloc       ntloc
       0.375       0.375          0.          0.           0           0
*SECTION_SOLID
$       SID      ELFORM         AET
          2          11
*SECTION_SOLID
$       SID      ELFORM         AET
          3          11
*SECTION_SOLID
$       SID      ELFORM         AET
         22          11           4
*SECTION_SOLID
$       SID      ELFORM         AET
         23          11           4
$
*PART
Air
$       PID       SECID         MID       EOSID        HGID        GRAV       ADAPT        TMID
          2           2           2           2           2           0
$
*PART
Water
$       PID       SECID         MID       EOSID        HGID        GRAV       ADAPT        TMID
          3           3           3           3           3           0
$
*PART
Air Reservoir
$       PID       SECID         MID       EOSID        HGID        GRAV       ADAPT        TMID
         22          22           2           2           2           0
$
*PART
Water Reservoir
$       PID       SECID         MID       EOSID        HGID        GRAV       ADAPT        TMID
         23          23           3           3           3           0
$
*PART
Tank Head
$       PID       SECID         MID       EOSID        HGID        GRAV       ADAPT        TMID
          6           6           6           0           6           0
Lift Ring & Cover
          9           9           9           0           9           0
Ballast Top Shell
         10          10          10           0          10           0
Bolting Ring
         11          11          11           0          11           0
Bolts
         12          12          12
Bolts
         14          14          14
$
$
*MAT_NULL
$       mid         rho          pc          mu       terod       cerod          ym          pr
          2    1.127E-7       -0.01
*MAT_NULL
$       mid         rho          pc          mu       terod       cerod          ym          pr
          3   9.3365e-5       -0.01   1.6300E-7   0.0000000   0.0000000
$*MAT_ELASTIC
$         6    0.000253      10.2E6        0.33
```

56

```
*MAT_PLASTIC_KINEMATIC
$       mid       rho         E        nu      sigy      etan      beta
          6    2.53E-4    10.2E6      0.33    18000.    10.2E4
$       src       srp        fs        vp

*MAT_ELASTIC
          9  0.000253    10.2E6      0.33
*MAT_ELASTIC
         10  0.000253    10.2E6      0.33
*MAT_ELASTIC
         11 0.0002491    10.2E6      0.33
*MAT_ELASTIC
         12  0.000733    29.6E6      0.30
*MAT_ELASTIC
         14  0.000733    29.6E6      0.30
$
$*EOS_IDEAL_GAS
$$    eosid        cv        cp        c1        c2        t0        v0
$         2    6.179E5   8.651E5       0.0       0.0    527.67       1.0
*EOS_LINEAR_POLYNOMIAL
$    eosid        c0        c1        c2        c3        c4        c5        c6
          2       0.0       0.0       0.0       0.0       0.4       0.4       0.0
$       e0        v0
      36.74       0.0
$
*EOS_LINEAR_POLYNOMIAL
$    eosid        c0        c1        c2        c3        c4        c5        c6
          3      14.7 3.11574e5 0.0000000 0.0000000 0.0000000 0.0000000
$       e0        v0
        0.0       0.0
$
*Hourglass
$     HGID       IHQ        QM
          2         1      1.E-6
          3         1      1.E-6
          6         8       0.1
          9         8       0.1
         10         8       0.1
         11         1       0.1
*SET_NODE_LIST_GENERATE
$      sid
       4111
$    b1beg     b1end
    4000001   4900000
*INITIAL_VELOCITY
$     nsid
       4111
$       vx        vy        vz       vxr       vyr       vzr
      96.26        0.        0.
*LOAD_BODY_X
          1    -386.1
*DEFINE_CURVE
          1         0       1.0       1.0       0.0       0.0         0
                        0.0       1.0
                      100.0       1.0
*SET_PART_LIST
$      sid
        781
$     pid1      pid2
          2         3
*INITIAL_HYDROSTATIC_ALE
$      SID   SIDTYPE     VECID   GRAVITY     PBASE
        781         0       789     386.1      14.7
$      NID  MMGBELOW
     103067         1
         44         2
*SET_PART_LIST
$      sid
        782
$     pid1      pid2
         22        23
*ALE_AMBIENT_HYDROSTATIC
$      SID   SIDTYPE     VECID   GRAVITY     PBASE
        782         0       789     386.1      14.7
$      NID  MMGBELOW
     103067         1
         44         2
```

```
*DEFINE_VECTOR
$       vid       xt       yt       zt       xh       yh       zh      cid
        789       0.       0.       0.       1.       0.       0.
$
*INCLUDE
water_mesh_rev1_reservoir.k
*DEFINE_TRANSFORMATION
        100
$                 a1       a2       a3       a4       a5       a6      a7
TRANSL          -7.9      0.0      0.0
$
*INCLUDE_TRANSFORM
run10c_tank_head_rev1.k
$   idnoff    ideoff    idpoff    idmoff    idsoff    idfoff    iddoff
    4000000   4000000
$   idroff

$   fctmas    fcttim    fctlen    fcttem    incout1
                                                  1
$   tranid
        100
$
*END
```

1. REPORT DATE *(DD-MM-YYYY)* 01-12-2014	2. REPORT TYPE Contractor Report		3. DATES COVERED *(From - To)* October 2013 - September 2014
4. TITLE AND SUBTITLE Elemental Water Impact Test: Phase 2 36-inch Aluminum Tank Head		5a. CONTRACT NUMBER NNL12AA09C	
		5b. GRANT NUMBER	
		5c. PROGRAM ELEMENT NUMBER	
6. AUTHOR(S) Vassilakos, Gregory J.		5d. PROJECT NUMBER	
		5e. TASK NUMBER	
		5f. WORK UNIT NUMBER 747797.06.13.06.32.04.03	
7. PERFORMING ORGANIZATION NAME(S) AND ADDRESS(ES) NASA Langley Research Center Hampton, Virginia 23681		8. PERFORMING ORGANIZATION REPORT NUMBER	
9. SPONSORING/MONITORING AGENCY NAME(S) AND ADDRESS(ES) National Aeronautics and Space Administration Washington, DC 20546-0001		10. SPONSOR/MONITOR'S ACRONYM(S) NASA	
		11. SPONSOR/MONITOR'S REPORT NUMBER(S) NASA/CR-2014-218667	

12. DISTRIBUTION/AVAILABILITY STATEMENT
Unclassified - Unlimited   Subject Category 31   Availability: NASA STI Program (757) 864-9658

13. SUPPLEMENTARY NOTES
Langley Technical Monitor: Robin C. Hardy

14. ABSTRACT
Spacecraft are being designed based on LS-DYNA simulations of water landing impacts. The Elemental Water Impact Test (EWIT) series was undertaken to assess the accuracy of LS-DYNA water impact simulations. EWIT Phase 2 featured a 36-inch aluminum tank head. The tank head was outfitted with one accelerometer, twelve pressure transducers, thee string potentiometers, and four strain gages. The tank head was dropped from heights of 1 foot and 2 feet. The focus of this report is the correlation of analytical models against test data. As a measure of prediction accuracy, peak responses from the baseline LS-DYNA model were compared to peak responses from the tests.

15. SUBJECT TERMS
Acceleration; Coupling stiffness; Impact; LS-DYNA; Landing; Mesh density; Simulation; Water

16. SECURITY CLASSIFICATION OF:			17. LIMITATION OF ABSTRACT	18. NUMBER OF PAGES	19a. NAME OF RESPONSIBLE PERSON STI Help Desk (email: help@sti.nasa.gov)
a. REPORT	b. ABSTRACT	c. THIS PAGE			19b. TELEPHONE NUMBER *(Include area code)*
U	U	U	UU	68	(757) 864-9658